IChemE

0263–8762/01/$10.00+0.00

Trans IChemE, Vol. 79, Part A, April 2001

SCALING UP BUBBLE COLUMN REACTORS WITH THE AID OF CFD

R. KRISHNA and J. M. VAN BATEN

Department of Chemical Engineering, University of Amsterdam, Amsterdam, The Netherlands

Bubble column reactors, used widely in industry, often have large column diameters (up to 6 m) and are operated at high superficial gas velocities (in the range of 0.1 to 0.4 m s^{-1}) in the churn-turbulent flow regime. Experimental work on bubble column hydrodynamics is usually carried out on a scale smaller than 0.3 m, at superficial gas velocities lower than 0.25 m s^{-1}. The extrapolation of data obtained in such laboratory scale units to the commercial scale reactors requires a systematic approach based on the understanding of the scaling principles of bubble dynamics and of the behaviour of two-phase dispersions in large scale columns. We discuss a multi-tiered approach to bubble column reactor scale up, relying on a combination of experiments, backed by Computational Fluid Dynamics (CFD) simulations for physical understanding. This approach consists of the following steps:

(a) description of single bubble morphology and rise dynamics (in this case both experiments and Volume-of-Fluid (VOF) simulations are used);
(b) modelling of bubble-bubble interactions, with experiments and VOF simulations as aids;
(c) description of behaviour of bubble swarms and the development of the proper interfacial momentum exchange relations between the bubbles and the liquid; and
(d) CFD simulations in the Eulerian framework for extrapolation of laboratory scale information to large-scale commercial reactors.

Keywords: bubble columns; flow regimes; scale up strategy; hold-up; bubble rise; bubble interactions; CFD.

INTRODUCTION

When a column filled with a liquid is sparged with gas, the bed of liquid begins to expand as soon as the gas is introduced. As the gas velocity is increased the bed height increases almost linearly with the superficial gas velocity, U, provided the value of U stays below a certain value U_{trans}. This regime of operation of a bubble column is called the homogeneous bubbbly flow regime. The bubble size distribution is narrow and a roughly uniform bubble size, generally in the range 1–7 mm, is found. When the superficial gas velocity U reaches the value U_{trans} coalescence of the bubbles takes place to produce the first fast-rising 'large' bubble. The appearance of the first large bubble changes the hydrodynamic picture dramatically. The hydrodynamic picture in a gas-liquid system for velocities exceeding U_{trans} is commonly referred to as the heterogeneous or churn-turbulent flow regime[1]. In the heterogeneous regime, small bubbles combine in clusters to form large bubbles in the size range 20–70 mm[2]. These large bubbles travel up through the column at high velocities (between 1–2 m s^{-1}), in a more or less plug flow manner[3]. These large bubbles churn up the liquid phase and because of their high rise velocities they account for a major fraction of the gas throughput[4]. Small bubbles, which co-exist with large bubbles in the churn-turbulent regime, are 'entrained' in the liquid phase and, as a good approximation, have the same back-mixing characteristics of the liquid phase. The two regimes are portrayed in Figure 1, which also shows qualitatively the variation of the gas hold-up ϵ as a function of the superficial gas velocity U. When the gas distribution is very good, the regime transition region is often characterised by a maximum in the gas hold-up[5]. The transition between homogeneous and churn-turbulent regime is often difficult to characterize and it is not prudent to design a reactor to operate in the transition zone. The estimation of the gas hold-up in the bubble column reactor of industrial scale is an important but extremely difficult task.

The gas hold-up varies significantly with liquid properties. See data in Figure 2 for air–paraffin oil (ρ_L = 795 kg m^{-3}; μ_L = 0.0029 Pa s; σ = 0.029 N m^{-1}), air–water (ρ_L = 1000; μ_L = 0.001; σ = 0.072) and air–Tellus oil (ρ_L = 862; μ_L = 0.075; σ = 0.028) measured in a column of 0.38 m diameter with a sintered plate distributor.

The gas hold-up appears to also depend on the column diameter. See data in Figure 3 for air–paraffin oil, air–water and air–Tellus oil measured in a columns of 0.1 and 0.38 m diameter, both with a sintered plate distributor. Literature correlations for the gas hold-up bubble columns show a wide spread in their capabilities to predict the variation with respect to U and with respect to the column diameter D_T.

Figure 4(a) compares air–water experimental data in a 0.38 m diameter column as a function of U with several literature correlations[6–12]. Only the Krishna-Ellenberger[3] correlation matches the data successfully but this is to be expected because their correlation was developed including the data set shown. Figure 4(b) compares air–water gas

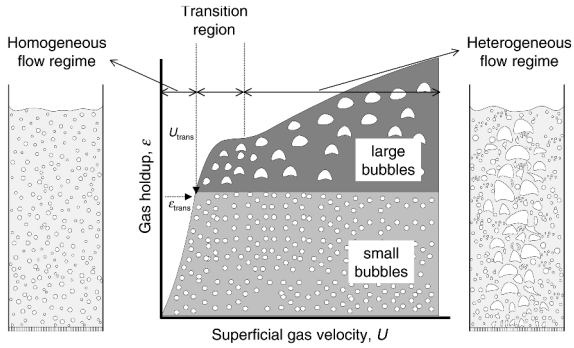

Figure 1. Homogeneous and churn-turbulent regimes in a gas-liquid bubble column.

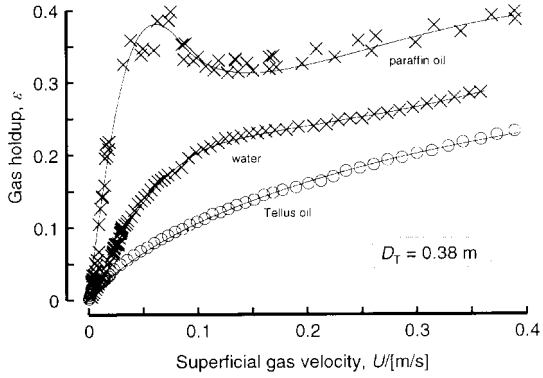

Figure 2. Comparison of the total gas hold-up measured in a column of 0.38 m internal diameter. Measurements with air-paraffin oil, air-water and air-Tellus oil.

hold-up predictions from different correlations as a function of column diameter for a constant superficial gas velocity $U = 0.2\ \mathrm{m\,s^{-1}}$. Only two correlations, those of Zehner[12] and Krishna and Ellenberger[3], predict a decline in ϵ with increasing column diameter D_T. For commercial processes column diameters should be extrapolated up to 6 m! Figures 5(a) and (b) present the corresponding information for air–Tellus oil; here we note that most literature correlations perform even worse than for the air–water system.

Clearly, a proper understanding of bubble hydrodynamics as a function of scale (column diameter and height) and physical properties of gas and liquid phases is needed before reliable procedures for scaling up a bubble column reactor of industrial size can be developed. So we start with trying to understand the behaviour of single gas bubbles in a liquid.

THE RISE CHARACTERISTICS OF GAS BUBBLES IN A LIQUID

The morphology and rise characteristics of a bubble depend strongly on the bubble size and system properties. A generalized graphical representation[13,14] of the rise characteristics is given in Figure 6 in terms of three dimensionless groups:

$$\text{Eötvös number, Eö} \equiv g(\rho_L - \rho_G)d_b^2/\sigma$$

$$\text{Morton number, M} \equiv g\mu_L^4(\rho_L - \rho_G)/(\rho_L^2\sigma^3)$$

$$\text{Reynolds number, Re} \equiv \rho_L d_b V_b^0/\mu_L$$

where d_b is the bubble diameter, taken to be equal to the diameter of a sphere with the same volume as that of the actual bubble, and V_b^0 is the rise velocity of a single, isolated, bubble. For the system air–water, $M = 2.63\times 10^{-11}$, $\log(\mathrm{M}) = -10.6$, we note that increasing the bubble size from around 4 mm (corresponding to Eö = 2.2) to 20 mm (Eö = 54.4) the regime changes from 'wobbling' to 'spherical cap'.

Bubble shapes and rise dynamics determined from Volume-of-Fluid simulations

The VOF model[15–26] resolves the transient motion of the gas and liquid phases using the Navier-Stokes equations, and accounts for the topology changes of the gas-liquid interface induced by the relative motion between the dispersed gas bubble and the surrounding liquid. The finite-difference VOF model uses a donor-acceptor algorithm, originally developed by Hirt and Nichols[19], to obtain, and maintain, an accurate and sharp representation of the gas-liquid interface. The VOF method defines a fractional volume or 'colour' function $c(\mathbf{x}, t)$ that indicates the fraction of the computational cell filled with liquid. The colour function varies between zero, if the cell is completely occupied by gas, and unity, if the cell consists only of the liquid phase. The location of the bubble interface is tracked in time by solving a balance equation for this function:

$$\frac{\partial c(\boldsymbol{x}, t)}{\partial t} + \nabla\cdot(\boldsymbol{u}c(\boldsymbol{x}, t)) = 0 \qquad (1)$$

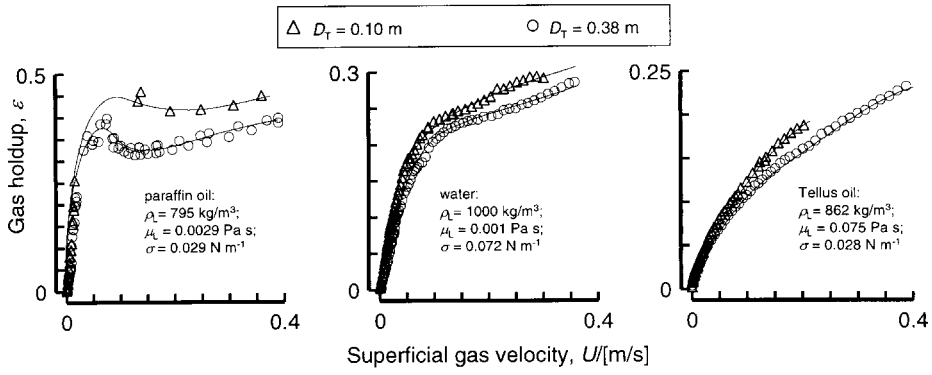

Figure 3. Comparison of the total gas hold-up measured in columns of 0.1 and 0.38 m internal diameters. Measurements with air-paraffin oil, air-water and air-Tellus oil.

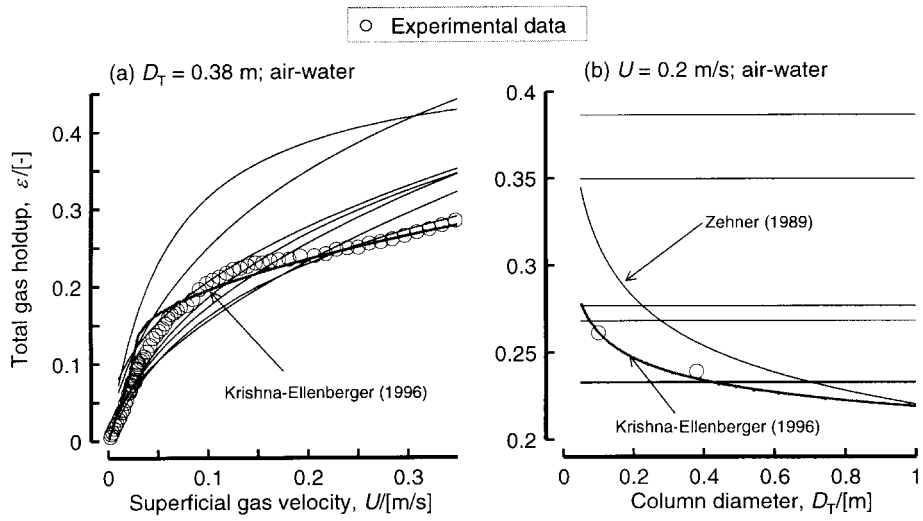

Figure 4. Comparison of literature correlations for the total gas hold-up ϵ for air-water system in column of 0.38 m diameter. (a) Variation of ϵ with superficial gas velocity for a column of 0.38 m diameter. (b) Variation of ϵ with column diameter for a superficial gas velocity of 0.2 m/s. The plotted correlations are from the literature[3,6–12].

The liquid and gas velocities are assumed to equilibrate over a very small distance and essentially $\boldsymbol{u}_k = \boldsymbol{u}$ for $k = L, G$ at the bubble interface. The mass and momentum conservation equations can be considered to be homogenous:

$$\nabla\cdot(\rho\boldsymbol{u}) = 0 \tag{2}$$

$$\frac{\partial\rho\boldsymbol{u}}{\partial t} + \nabla\cdot(\rho\boldsymbol{u}\boldsymbol{u}) = -\nabla p - \nabla\cdot\tau + \rho\boldsymbol{g} + \mathbf{F}_{sf} \tag{3}$$

where p is the pressure, τ is the viscous stress tensor, $\mathbf{G}$ is the gravitational force. The density and viscosity used in Equations (2) and (3) are calculated from

$$\rho = \epsilon_L\rho_L + \epsilon_G\rho_G; \quad \mu = \epsilon_L\mu_L + \epsilon_G\mu_G \tag{4}$$

where ϵ_k denotes the volume fraction of the phase $k = L, G$. The continuum surface force model, originally proposed by Brackbill *et al.*[27], is used to model the force due to surface tension acting on the gas-liquid interface. In this model the surface tension is modelled as a body force $\mathbf{F}_{sf}$, that is non-zero only at the bubble interface and is given by the gradient of the colour function:

$$\mathbf{F}_{sf} = \sigma\kappa(\boldsymbol{x})\nabla c(\boldsymbol{x}, t) \tag{5}$$

where $\kappa(\boldsymbol{x})$ is the local mean curvature of the bubble interface:

$$\kappa(\boldsymbol{x}, t) = \frac{1}{|\boldsymbol{n}|}\left(\left(\frac{\boldsymbol{n}}{|\boldsymbol{n}|}\cdot\nabla\right)|\boldsymbol{n}| - \nabla\cdot\boldsymbol{n}\right) \tag{6}$$

where $\boldsymbol{n}$ is the vector normal to the bubble interface:

$$\boldsymbol{n} = \nabla c(\boldsymbol{x}, t) \tag{7}$$

The Equations (1)–(7) have been solved using dedicated[15–18] or commercially available codes[20–26]. The VOF simulations of Krishna and Van Baten[21–24] for a two-dimensional rectangular column filled with water into which bubbles of various sizes were 'inserted' are shown in

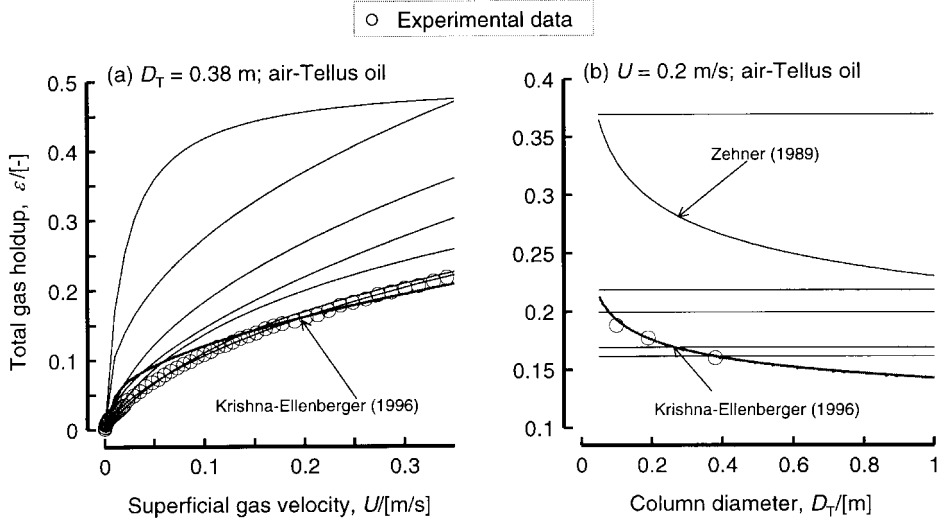

Figure 5. Comparison of literature correlations and experimental data for the total gas hold-up ϵ for air-Tellus oil system in column of 0.38 m diameter. Variation of ϵ with superficial gas velocity for a column of 0.38 m diameter. (b) Variation of ϵ with column diameter for a superficial gas velocity of 0.2 m/s. Same correlations[3,6–12] as specified in the legend to Figure 4.

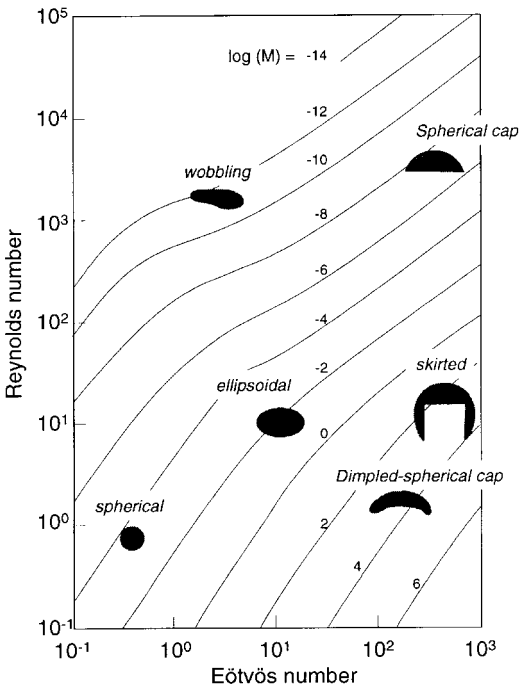

Figure 6. Shape regimes for bubble rising in a column of liquid. Adapted from Clift, Grace and Weber[13].

Figure 7. The 4 and 5 mm bubbles show meandering trajectories. The 7 mm bubble oscillates from side to side when moving up the column. The 9 mm bubble behaves like a jellyfish. The 12 mm bubble flaps its 'wings' like a bird. The 20 mm bubble assumes a spherical cap shape and has a vertical rise trajectory. These rich dynamic features can be viewed by looking at the animations on the web site: http://ct-cr4.chem.uva.nl/single_bubble/. As the bubble size increases, the amplitude of the excursions in the x-directions decrease; see Figure 8.

From the VOF simulations shown in Figure 7, the transition between wobbling ellipsoidal-shaped bubble and the spherical-cap bubbles appears to proceed gradually via a scala of shapes and rise characteristics. The jellyfish and bird-like motions of the bubbles are particularly intriguing. In order to verify these, we tracked the rise characteristics of air bubbles in a 2D rectangular column of water, similar to the one used in our earlier study[2]. The column was made up of two parallel glass plates 0.3 m wide and 4 m high. The distance between the glass plates was 5 mm. Provision was made to inject gas bubbles via a central tube of 2 mm diameter in the distributor. The bubble trajectories were recorded on video at 25 frames per second[23]. The re-traced video images for bubbles of 9.7, 12.3, 13.7 and 15.5 mm in size are shown in Figure 9. The 9.7 mm bubble exhibits jellyfish like characteristics. Close observation of the edges of the 13.7 mm bubble confirms the vertical

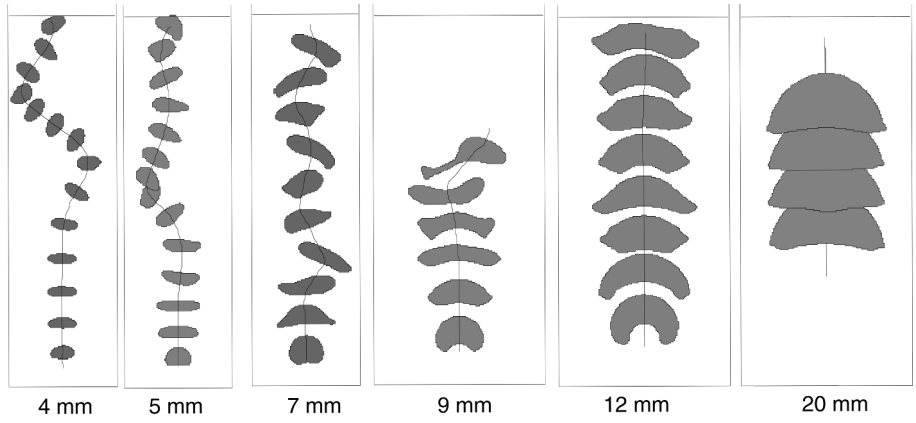

Figure 7. Snapshots obtained with two-dimensional VOF simulations of the rise trajectories of bubbles in the 4–12 mm size range. Animations of all these VOF simulations can be viewed on our web site http://ct-cr4.chem.uva.nl/single_bubble

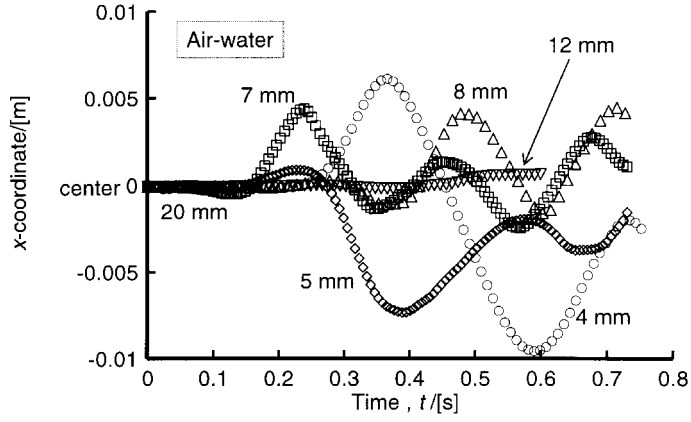

Figure 8. Comparison of the x-trajectories obtained with two-dimensional VOF simulations of bubbles in the 4–20 mm size range.

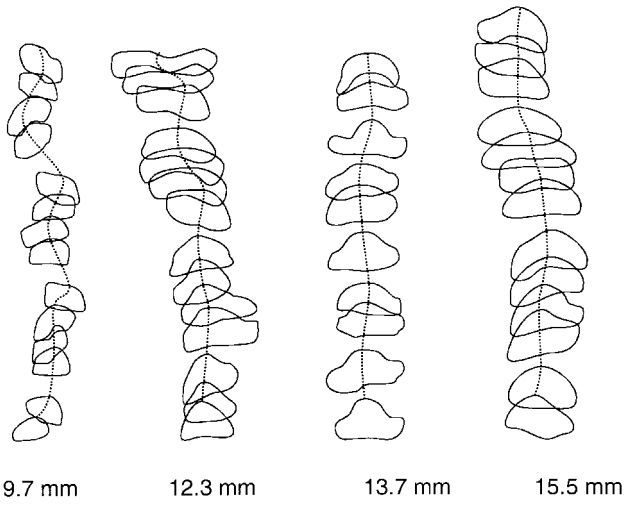

Figure 9. Retraced video recordings of the rise characteristics of 9.7, 12.3, 13.7 and 15.5 mm bubbles observed in a 2D rectangular column. Experimental data from[23].

oscillation, analogous to the flapping of the wings of a bird. When the bubble size increases to 15.5 mm, these vertical oscillations vanish. Furthermore, our video recordings also show that the excursions in the x-direction decreases with increasing bubble size, in confirmity with the VOF results of Figure 7.

Having obtained qualitative confirmation of the VOF simulations as regards bubble shape and morphology, the next step is to see if the rise velocities calculated from the VOF simulations conform to experiment. The rise velocities of the bubbles in the 4–12 mm size range, determined from the average z-distance covered per unit time from the VOF simulations, have been compared with measured data for this size range in the 0.174 and 0.63 m diameter columns of cylindrical cross-section by Krishna *et al.*[20,22,24]. The experimental data of Krishna *et al.*[20,22,24] conform quite well with the correlation of Harmathy[28]:

$$V_b^0 = 1.53\left(\frac{\sigma g}{\rho_L}\right)^{0.25} \tag{8}$$

The Harmathy correlation for the bubble rise velocity shows this to be independent of the bubble diameter for the size range considered. Both VOF simulations and experiments confirm only a weak dependence of V_b^0 on the bubble diameter. The 2D VOF simulations give rise velocity values that are roughly half those measured experimentally in cylindrical columns. The VOF simulations were carried out in two-dimensional columns with a maximum width of only 0.04 m; the bubble rise is therefore significantly influence by wall effects. A complete three-dimensional simulation would be required to determine the rise velocity quantitatively; such a simulation would require a grid with a few million grid cells and the use of a massively parallel computer.

VOF simulations can only provide a qualitative understanding of bubble morphology and rise characteristics. In particular the transition from 'wobbling' to 'spherical cap' regime for water in Figure 6 is seen to be a smooth one proceeding through a variety of intermediate regimes.

Behaviour of Swarms of 'Small' Bubbles

Consider the homogeneous regime of operation in an air-water system containing a swarm of 'small' bubbles. A single small bubble in this size range exhibits lateral movement as shown in Figures 7 and 8. The behaviour of a swarm of such bubbles is interesting because the lateral motion of each bubble affects the neighbouring bubble. The result swarm motion is best appreciated by viewing the animations of VOF simulations of a swarm of 5 mm bubbles in a column of water carried out by Krishna and Van Baten[24]. Snapshots of these simulations are shown in Figure 10. For 5-mm sized bubbles we have a small, closed, wake[14] and there are not wake interactions between bubbles. Each bubble in the swarm tends to 'avoid' each other. This 'avoidance' can also be viewed as mutual 'hindering' of the rise velocity. In the chemical engineering literature, the hindered rise of gas bubbles is described by the Richardson-Zaki[29] relation:

$$V_b = V_b^0(1-\epsilon)^{n-1} \tag{9}$$

where the bubble swarm velocity V_b^0 is obtained by 'correcting' the single bubble rise velocity V_b^0 for the finite gas hold-up of the gas bubbles, ϵ. The exponent n is the Richardson-Zaki index and for air bubbles in water has a value of about 2, i.e. $n \approx 2$. As the gas hold-up ϵ increases, the bubble swarm velocity decreases. For a gas hold-up $\epsilon = 0.1$, the decrease in the bubble swarm velocity about 10% when compared to the single bubble value V_b^0.

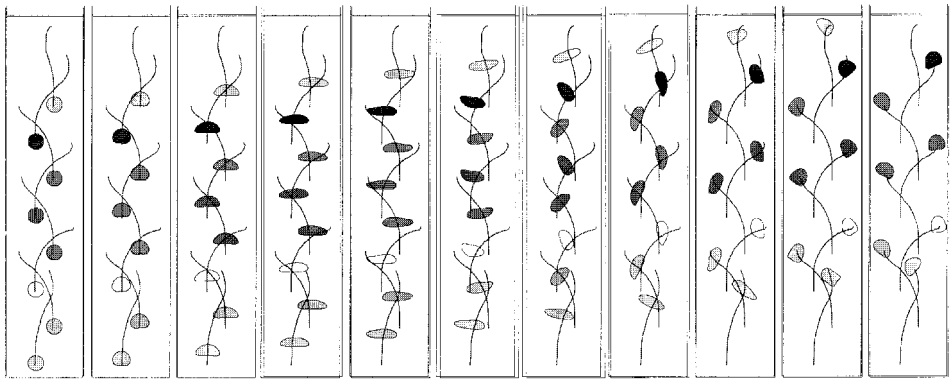

Figure 10. Rise trajectories of a swarm of 5 mm bubbles, eight in number, in a column of water. Animations of all these VOF simulations can be viewed on the web site http://ct-cr4.chem.uva.nl/single_bubble

Rise Characteristics of a Single Spherical Cap Bubble

For values of Eö > 40 (for air-water system, this corresponds to bubble sizes larger than 17 mm), bubbles assume a spherical cap shape as seen in Figures 6 and 7. The rise velocity of spherical cap bubbles is given by the classic Davies and Taylor[30] relationship:

$$V_b^0 = \sqrt{gd_b/2} = 0.71\sqrt{gd_b} \tag{10}$$

The relationship (10) is remarkable in that the velocity rise does not depend on the physical properties of either the liquid or gas. The Davies-Taylor relationship Equation (10) is found to be applicable provided the ratio $d_b/D_T < 0.125$. For values of d_b/D_T exceeding 0.125, Collins[31] introduced a scale correction factor, SF, into the Davies-Taylor relationship:

$$V_b^0 = 0.71\sqrt{gd_b}(SF) \tag{11}$$

This scale correction factor was determined empirically to be given by Collins[31] as follows:

$$SF = 1 \qquad \text{for } \frac{d_b}{D_T} < 0.125$$

$$SF = 1.13\exp\left(-\frac{d_b}{D_T}\right) \qquad \text{for } 0.125 < \frac{d_b}{D_T} < 0.6$$

$$SF = 0.496\sqrt{D_T/d_b} \qquad \text{for } \frac{d_b}{D_T} > 0.6 \tag{12}$$

The conditions wherein $d_b/D_T > 0.6$ corresponds to the special case of slug flow for which the bubble rise velocity is independent of the bubble diameter and is given by

$$V_b^0 = 0.35\sqrt{gD_T} \tag{13}$$

The Davies-Taylor-Collins relations Equations (10)–(13) also hold for bubble rise in gas-solid fluidized beds of powders[32].

Extensive experiments carried out by Krishna *et al.*[20,22] in four different columns of diameters 0.051, 0.1, 0.174 and 0.63 m, with the air-water system confirm the validity of the Davies-Taylor-Collins relations Equations (11) and (12); see Figure 11. The strong influence of the scale factor on the rise velocity is emphasised when we consider the rise of a bubble of 0.038 m diameter as a function of column diameter; see Figure 12. In the 0.051 m diameter column we have slugging (cf. Equation (13)) and the bubble rise velocity is 0.25 m s^{-1}. For the 0.1 m diameter column the rise velocity is 0.34 m s^{-1}, increasing to 0.44 m s^{-1} in the 0.63 m diameter column.

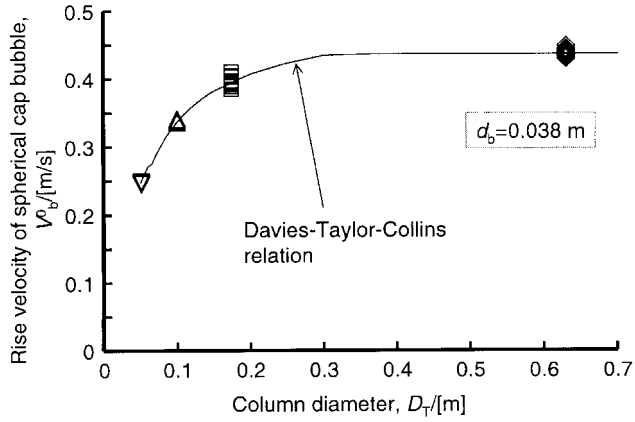

Figure 12. Rise velocity of spherical cap bubble of 0.038 m diameter as a function of the column diameter.

VOF simulations, assuming cylindrical axi-symmetry, have been used by Krishna *et al.*[20] to provide a physical understanding of the scale (wall) effects for spherical cap bubbles. Plotted in Figure 13 are z-coordinates of the nose of 21 mm bubbles rising in columns of 0.1 and 0.051 m diameters filled with water obtained from VOF simulations. Figure. 13 clearly shows that the bubble rises faster in the wider column. The reason for this is the restraining effect of the walls. The insets to Figure 13 show the liquid phase velocity profiles for these two simulations. The 21 mm bubble assumes a flatter shape in the 0.1 m wide column and is less influenced by the wall than the same bubble placed in a 0.051 m wide column. Put another way, the drag between the bubble and the liquid is higher in the narrower column due to the higher downward liquid velocity in the vicinity of the bubble. For spherical cap bubbles, axi-symmetric VOF

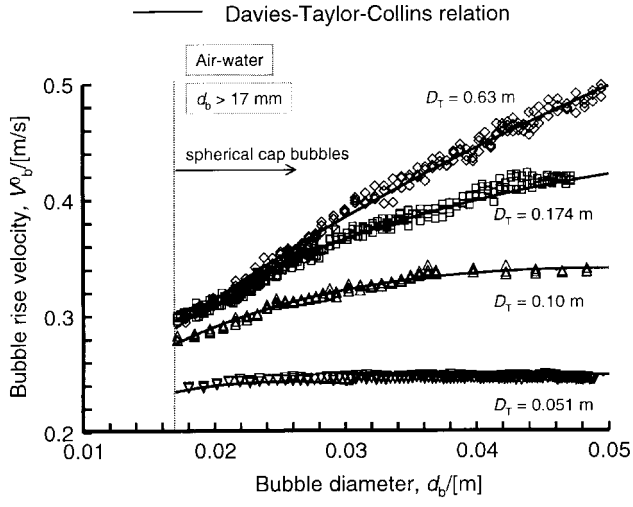

Figure 11. Rise velocity of air bubbles of varying diameters in columns of 0.051, 0.1, 0.174 and 0.63 m diameter filled with water; comparison of experimental data with the predictions of the Davies-Taylor-Collins Equations (11) and (12).

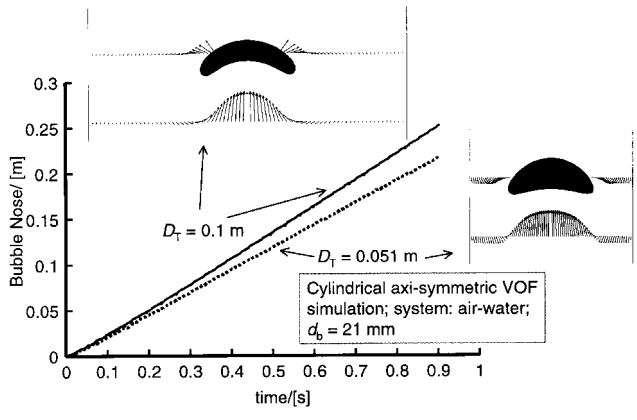

Figure 13. VOF simulations of the rise trajectories of a 21 mm diameter bubble in 0.051 and 0.1 m diameter columns. The insets show the liquid phase velocity profiles surrounding the bubble. Animations of these VOF simulations can be viewed on the web site http://ct-cr4.chem.uva.nl/axissym

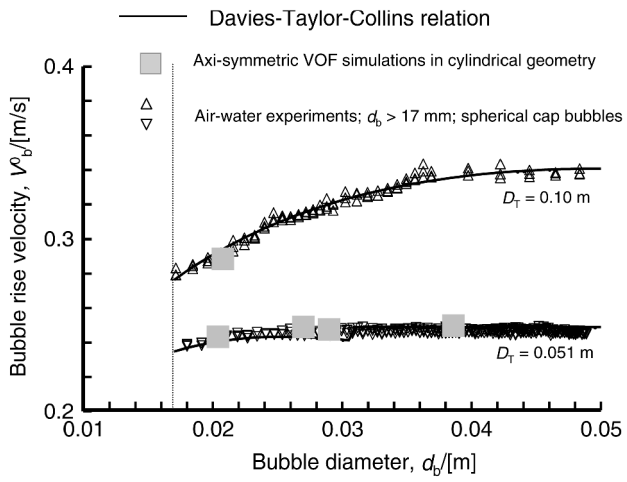

Figure 14. Rise velocity of air bubbles of varying diameters in columns of 0.051 and 0.1 m diameter columns filled with water. Comparison of experimental data with the predictions of the Davies-Taylor-Collins Equations (11) and (12) and VOF simulations.

simulations yield values of the rise velocity that are in excellent agreement with measured experimental data; see Figure 14. They provide a physical explanation of wall effects embodied in the Davies-Taylor-Collins relations Equations (11) and (12).

In further discussions on the subject of bubble columns, we shall be talking about 'small' and 'large' bubbles. Roughly speaking, 'small' bubbles are taken to represent bubbles smaller than about 10 mm. 'Large' bubbles are taken to correspond to the requirement of Eö > 40, corresponding to sizes larger than about 17 mm. It is important to distinguish between these bubble classes because 'small' bubbles have morphologies and rise characteristics that are significantly affected by system properties. 'Large' bubbles on the other hand are relatively insensitive to system properties. The rise characteristics of large bubbles are however significantly affected by scale as demonstrated in this section.

Rise Velocity of Circular Cap Bubbles in Two-dimensional Columns

Experimental work to study bubbling behaviour and hydrodynamics is often carried out using two-dimensional rectangular gas-liquid bubble columns[2] and two-dimensional rectangular gas-solid fluidised beds[25,33,34]. A typical experimental set-up is shown in Figure 15. In order to be able to translate the information from 2D beds to columns of cylindrical cross-section, it is important to be able to interrelate the single bubble rise velocity in these two column configurations.

In Figure 16 we show experimental measurements of the rise velocities of 2D circular cap bubbles in water, silica and polystyrene in a 0.3 m diameter column[25]. We see that the Froude number, $V_b/\sqrt{gd_b}$, appear to decrease significantly with increasing value of the ratio of the bubble diameter to column width, d_b/D_T; see Figure 16(a). The experimental data lie about 10–30% below the values calculated from the Davies-Taylor-Collins Equations (11) and (12). Based on the experimental data alone, it is not possible to set up a relation to parallel Equations (11) and (12) because the

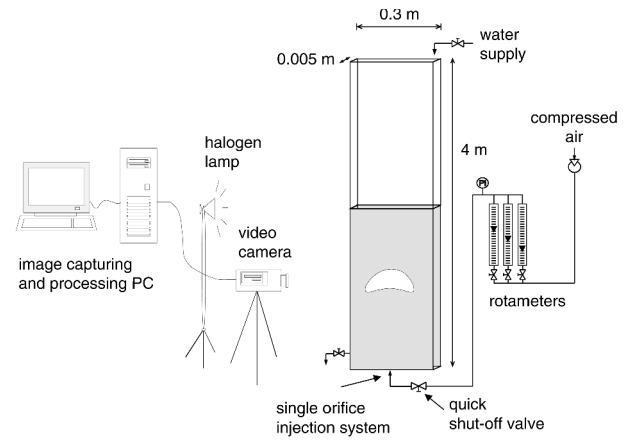

Figure 15. Typical experiment set-up for measurement of rise velocities of single gas bubbles in water and in fluidized beds[2,25].

range of d_b/D_T values in the experiments is restricted to below 0.5.

Two-dimensional VOF simulations in Cartesian geometry for a variety of bubble sizes in columns of varying width can be used to supplement to experimental data; see Figure 16(b). The 2D VOF simulations, and experiments in 2D rectangular columns, can be combined to yield the following 2D analogue of the Davies-Taylor-Collins relations:

$$V_b = 0.62\sqrt{gd_b}(SF) \tag{14}$$

with the scale factor given by

$$\begin{aligned} SF &= 1 && \text{for } \frac{d_b}{D_T} < 0.07 \\ SF &= 1.1\exp\left(-1.55\frac{d_b}{D_T}\right) && \text{for } 0.07 < \frac{d_b}{D_T} < 0.4 \\ SF &= 0.38\sqrt{D_T/d_b} && \text{for } \frac{d_b}{D_T} > 0.4 \end{aligned} \tag{15}$$

Equations (14) and (15) hold equally for the bubble rise

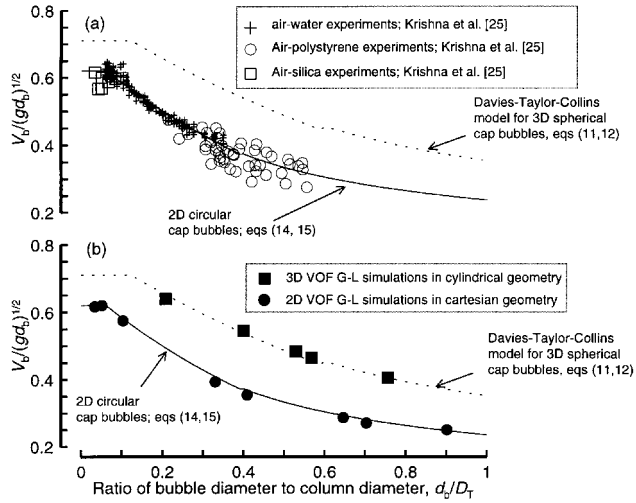

Figure 16. (a) Bubble rise velocities in two-dimensional rectangular columns. Experimental data in 2D rectangular column (cf. Figure 15). (b) 2D and 3D VOF simulations.

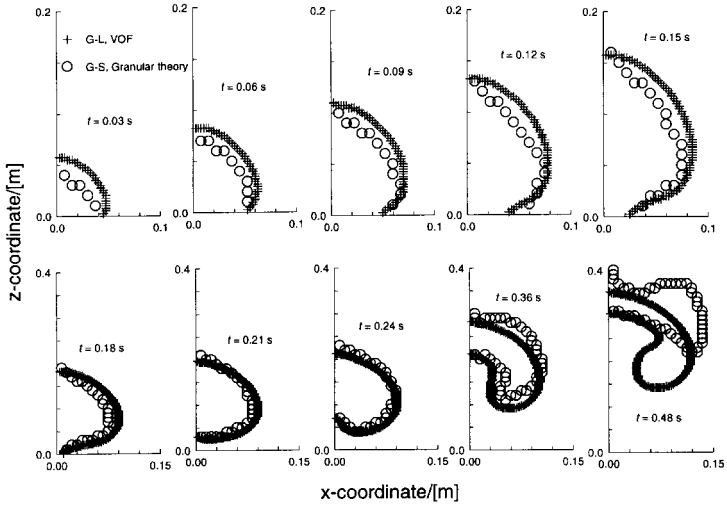

Figure 17. Snapshots of the simulation of the formation of a gas bubble in a gas-solid fluidised bed of powder and water carried out respectively with the granular theory and VOF technique. A gas jet enters a 0.57 m wide rectangular fluid bed consisting of water or a powder of mean particle size of 500 μm with a skeletal density of 2660 kg m^{-3}. The gas jet enters the bed with a velocity of 10 m s^{-1} and is maintained for 0.18 s from the start of gas injection. The system geometry is the same as the one used by Kuipers *et al.*[40]. Note the change in the scales between the upper and bottom rows. For a gas-solid system the contours of a bubble are defined by the requirement that the voidage is greater than 0.85. Animations of these simulations can be viewed on our web site http://ct-cr4.chem.uva.nl/analogies

velocity in 2D rectangular columns filled with a liquid or powder.

In order to provide further verification of the conclusion that the rise velocity of circular-cap bubbles in 2D gas-solid and gas-liquid systems is described by an identical relationship let us compare CFD simulations of a the formation and rise of a single gas bubble in a 2D rectangular gas-solid fluidised bed and in an identical bed filled with water. For simulation of a gas-solid system, the kinetic theory of granular flow was used [35–43]. The granular theory simulations are shown in Figure 17 along with 2D VOF simulations with the air-water system. The equivalence of the bubble formation and rise phenomena is evident in the initial stages. For a gas-solid system there is no surface tension and the bubble break-up phenomenon is different; this is evident towards the latter stages of bubble rise (see snapshot at $t = 0.48$ s). The time trajectories of the nose of the bubble in Figure 17 are compared in Figure 18. It is clear that the rise velocity is identical in the initial stage of bubble rise.

The results in Figures 17 and 18 underlines the analogies in the bubble rise phenomena in powders and liquids and goes some way in explaining the reason behind the applicability of Equations (11)–(15) to both gas-liquid systems and gas-solid systems[32]. We shall demonstrate later in this paper that the analogies can be exploited to develop an analogous scale up strategy for gas-solid fluidized beds.

In-line Interaction of a Pair of Spherical Cap Bubbles

The next step in the understanding of bubble column hydrodynamics is to consider in-line interaction between two 'large' spherical cap bubbles. Consider two bubbles of the same size $d_b = 31$ mm, separated vertically in a 0.051 m diameter column (see video images of this experiment in Figure 19). The trailing bubble is accelerated and gets sucked into the wake of the leading bubble. It is clear that the acceleration effect increases as the trailing bubble approaches the leading bubble. The VOF simulation of Krishna *et al.*[20] of this experiment is shown in Figure 20. The reason that the shape of the bubbles in the VOF simulations appears to be hollower than in the experiment is due to the fact that in the video recordings only the outer periphery of the bubbles can be visualised. The contours of the bubbles in Figure 20, on the other hand, are drawn for a

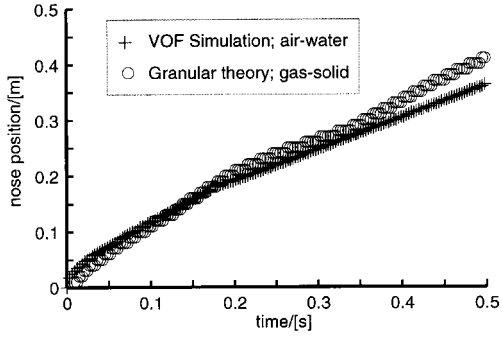

Figure 18. Comparison of the rise trajectories of the bubble in the granular and VOF simulations shown in Figure 17.

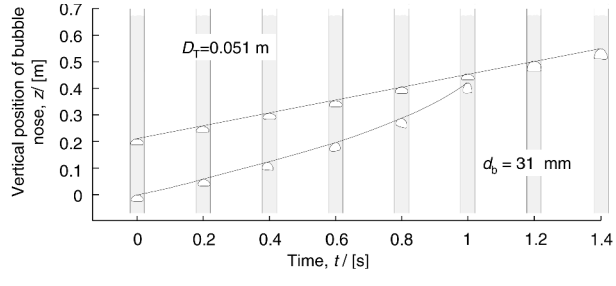

Figure 19. Retraced video images of in-line interactions of 31 mm diameter bubbles rising in a 0.051 m diameter column filled with water.

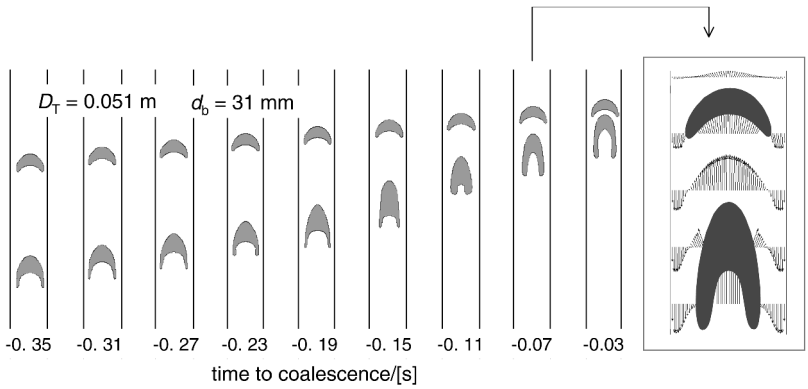

Figure 20. VOF simulations, using cylindrical axi-symmetry, of the experiment shown in Figure 19. The inset shows the liquid phase velocity profiles for the situation corresponding to 0.07 s before coalescence. An animation of this VOF simulation can be viewed on the web site http://ct-cr4.chem.uva.nl/axissym

slice in the r–z plane. The liquid phase velocity profiles at 0.07 s before coalescence of the bubbles are indicated in the inset in Figure 20. A comparison of the measured trajectories for both leading and trailing bubbles with VOF simulations shows very good agreement; see Figure 21.

VOF simulations provide a physical understanding of the in-line interactions of large spherical cap bubbles. Such interaction leads to an acceleration of the trailing bubble. The acceleration factor AF increases as the trailing bubble approaches closer to the leading bubble; see experimental data in Figure 22. This acceleration effect needs to be accounted for when modelling a swarm of large bubbles in a bubble column operating in the churn-turbulent regime. The large bubble swarm velocity can therefore be expected to be much higher than that of a single, isolated, bubble, V_b^0. We therefore assert that

$$V_b = V_b^0(AF) \tag{16}$$

for a swarm of 'large' spherical cap bubbles in a liquid. It is interesting to note that while 'small' bubbles suffer hindrance in a swarm, large bubbles experience acceleration.

In large diameter columns, both in-line and out-of-line interactions of bubbles can take place and the precise mechanisms of bubble coalescence are discussed by Krishna *et al.*[20].

Estimation of Large Bubble Swarm Velocity in Bubble Columns

The acceleration factor AF determined from experiments shown in Figure 22 is valid for a bubbling trailing another bubble. We need to extend this concept to a swarm of 'large' bubbles in a bubble column operating in the churn-turbulent regime. For this purpose we first consider a simplified picture of the hydrodynamics in this regime, put forward by Krishna and Ellenberger[3,4,44–46]; see Figure 23. The dispersion is assumed to consist of two bubble classes: small and large. The dynamic gas disengagement technique allows the experimental determination of the gas holdups in the large and small bubble populations[3]. The superficial gas velocity through the small bubble population is assumed to equal that at the regime transition point, U_{trans}. The remainder of the entering gas flows up the column in the form of large bubbles. The superficial gas velocity through the large bubble 'phase' is therefore $(U - U_{trans})$. For steady-state mode of operation in the churn-turbulent regime, every 'large' bubble is a 'trailing' bubble because

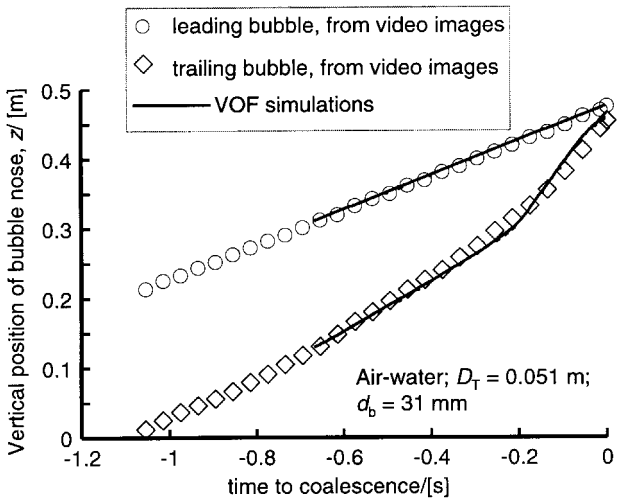

Figure 21. Comparison between experiment and VOF simulation of the rise trajectories of the leading and trailing bubbles in a 0.051 m diameter column filled with water.

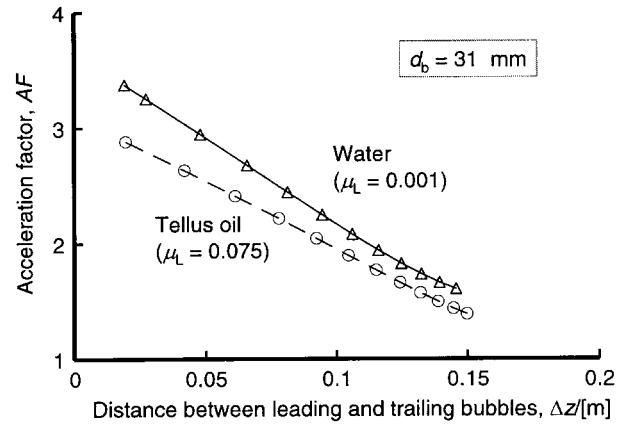

Figure 22. The acceleration factor for the trailing bubble as function of its distance of separation from the preceding bubble. The measurements with Tellus oil were made in a 0.1 m diameter column and those with water were made in a 0.051 m diameter column.

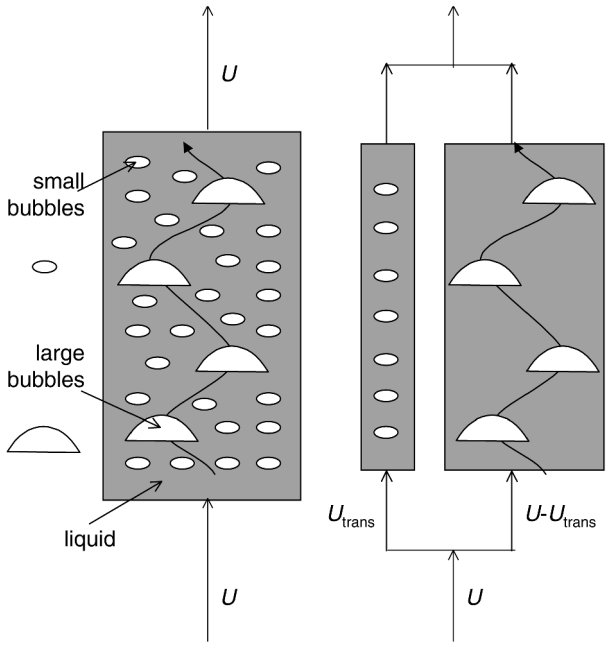

Figure 23. Three-phase model for bubble columns operating in the churn-turbulent regime.

there will be a bubble preceding it. The large bubble swarm velocity can therefore be expected to be much higher than that of a single, isolated, bubble V_b^0. From the data in Figure 22, we should expect the acceleration factor AF to increase linearly with decreasing distance of separation of the bubbles. With increasing values of $(U - U_{trans})$ we should expect the average distance of separation between the large bubbles to decrease. We therefore assert that:

$$V_b = V_b^0(AF); \quad AF = \alpha + \beta(U - U_{trans}) \tag{17}$$

where V_b^0 is given by Equations (11) and (12). The experimental data on the large bubble swarm velocity V_b as a function of $(U - U_{trans})$ reported in Krishna and Ellenberger[3,4] comprising of more than 1000 measured points with liquids of relatively low viscosity (less than 0.0029 Pa s) were used to obtain the following expressions for the average large bubble diameter

$$d_b = 0.069(U - U_{trans})^{0.376} \tag{18}$$

and the acceleration factor, AF:

$$AF = 2.73 + 4.505(U - U_{trans}); \quad \text{for low viscosity liquids} \tag{19}$$

The fitted bubble size correlation (Equation 18) matches very well with the measured bubble size data of De Swart *et al.*[2]; see Figure 24. In Figure 25 we compare the experimental values of the large bubble swarm velocity V_b for the air-water system measured in three different columns with the predictions of Equations (11), (12), (17), (18) and (19).

From the large bubble swarm velocity measurements made with the system air–Tellus oil[20], the corresponding fit for the acceleration factor is

$$AF = 2.25 + 4.09(U - U_{trans}); \quad \text{for Tellus oil} \tag{20}$$

while the fit for the bubble size d_b remains the same as for 'low' viscosity liquids, i.e. equation (18). Figure 25 testifies to the goodness of the fit.

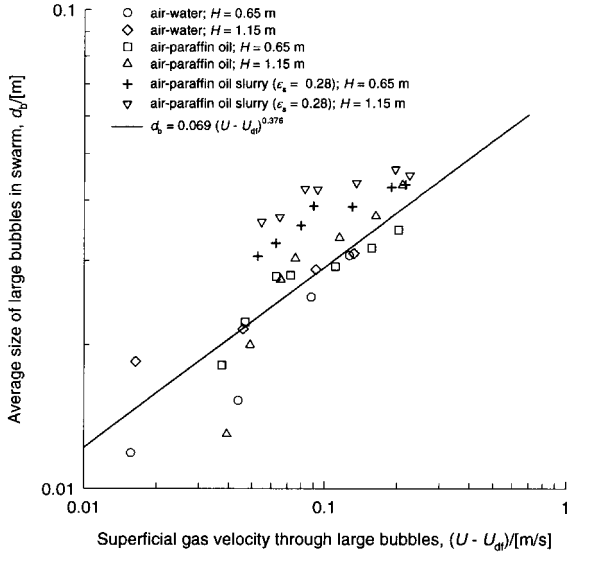

Figure 24. Correlation for the average bubble size of large bubble swarm as function of the superficial gas velocity through the large bubble population. The experimental data is from Krishna *et al.*[2,55], measured with the systems air-water and air-paraffin oil in a 2D rectangular column of 0.3 m width at different heights H above the distributor.

EULERIAN SIMULATION MODEL FOR BUBBLE COLUMNS

There has been considerable activity in recent years in the development of CFD model for bubble columns. Most authors have adopted the Eulerian description of the bubble and liquid phases, considering these as two, interpenetrating, phases[47–64]. A few authors have chosen the Lagrangian description of the bubbles, treating these as discrete particles[65,66]. From considerations of computer load, only the Eulerian–Eulerian two-phase model is suitable for the purpose of design and scale up of individual reactors. Our focus in this paper is on industrial scale bubble columns with aspect ratios greater than say five, operating at high gas velocities in the churn-turbulent flow regime. For the cases under consideration, the influence of the gas distribution device will be negligibly small[3].

For each of the three phases shown in Figure 23 the volume-averaged mass and momentum conservation equations in the Eulerian framework are given by:

$$\frac{\partial(\epsilon_k\rho_k)}{\partial t} + \nabla\cdot(\rho_k\epsilon_k\boldsymbol{u}_k) = 0 \tag{21}$$

$$\frac{\partial(\rho_k\epsilon_k\boldsymbol{u}_k)}{\partial t} + \nabla\cdot(\rho_k\epsilon_k\boldsymbol{u}_k\boldsymbol{u}_k - \mu_k\epsilon_k(\nabla\boldsymbol{u}_k + (\nabla\boldsymbol{u}_k)^T)) = -\epsilon_k\nabla p + \mathbf{M}_{kl} + \rho_k\boldsymbol{g} \tag{22}$$

where ρ_k, $\boldsymbol{u}_k$, ϵ_k and μ_k represent, respectively, the macroscopic density, velocity, volume fraction and viscosity of the kth phase, p is the pressure, $\mathbf{M}_{kl}$, the interphase momentum exchange between phase k and phase l and $\boldsymbol{g}$ is the gravitational force.

The momentum exchange between either bubble phase

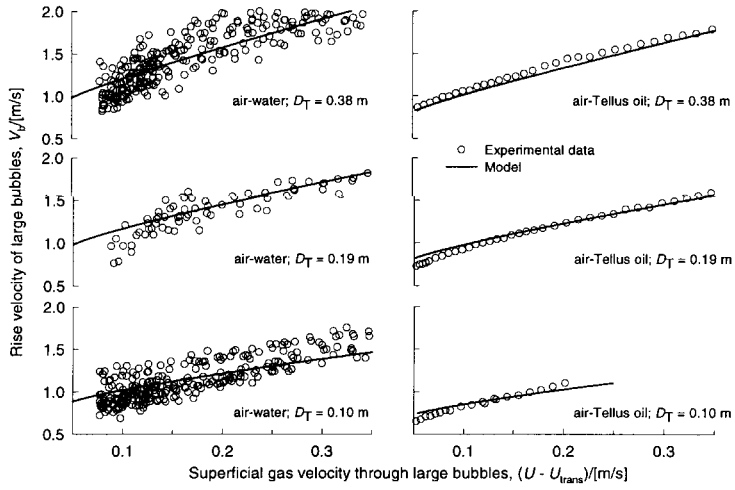

Figure 25. Comparison of model for large bubble swarm velocity given by Equations (11), (12), (17)–(20) with air-water measurements (left figure) and air-Tellus oil measurements (right figure) in columns of 0.1, 0.19 and 0.38 m diameter.

(subscript b) and liquid phase (subscript L) phases is given by:

$$\mathbf{M}_{L,b} = \frac{3}{4}\rho_L \frac{\epsilon_b}{d_b} C_D(\boldsymbol{u}_b - \boldsymbol{u}_L)|\boldsymbol{u}_b - \boldsymbol{u}_L| \tag{23}$$

The liquid phase exchanges momentum with both the 'small' and 'large' bubble phases. No interchange between the 'small' and 'large' bubble phases have been included in the present model and each of the dispersed bubble phases exchanges momentum only with the liquid phase. The neglect of the interactions between the small and large bubble populations is due to the conclusion reached by Vermeer and Krishna[67]. The interphase drag coefficient is calculated from equation:

$$C_D = \frac{4}{3}\frac{\rho_L - \rho_G}{\rho_L} g d_b \frac{1}{V_b^2} \tag{24}$$

where V_b is the rise velocity of the appropriate bubble population. For the small bubble population, the bubble rise velocity V_b can be estimated from the Harmathy relation (Equation 8). Since the rise velocity of 'small' bubbles is relatively insensitive to the bubble diameter, the final results are also relatively insensitive to the choice of the bubble diameter. The large bubble swarm velocity V_b is estimated using the procedure outlined earlier, properly accounting for bubble-bubble interactions.

The drag force contribution to $\mathbf{M}_{L,b}$ is the dominant one[61,63]. In the literature other contributions to $\mathbf{M}_{L,b}$ such as added mass and lift force have also been considered[51]. The concept of added mass does not hold for 'large' bubbles because these bubbles do not have a closed wake. There is considerable uncertainty in assigning values of the lift coefficients to the small and large bubbles. For the large bubbles, for which Eö > 40 holds, data suggest the use of a negative lift coefficient, whereas for small bubbles for which typically Eö = 2, the lift coefficient is positive[51]. In the simulation results presented below only the drag force contribution to $\mathbf{M}_{L,b}$ is considered.

For the continuous (liquid-) phase, the turbulent contribution to the stress tensor is evaluated by means of k–ϵ model, using standard single phase parameters $C_\mu = 0.09$, $C_{1\epsilon} = 1.44$, $C_{2\epsilon} = 1.92$, $\sigma_k = 1$ and $\sigma_\epsilon = 1.3$. The applicability of the k–ϵ model has been considered in detail by Sokolichin and Eigenberger[63]. No turbulence model is used for calculating the velocity fields inside the dispersed 'small' and 'large' bubble phases. In this paper we shall compare macroscopic experimental data on gas holdup, velocity profiles, dispersion of phases with Eulerian simulations; for this purpose, the k–ϵ model appears to be adequate.

2D AXI-SYMMETRIC SIMULATIONS

We simulated the following three sets of experiments.

- Air-water experiments of Hills[68] carried out in a column of 0.14 m diameter;
- Air-water experiments of Krishna *et al.*[52] carried out in columns of 0.174, 0.38 and 0.63 m diameter; and
- Air–Tellus oil experiments of Krishna *et al.*[53,54] in columns of 0.1, 0.19 and 0.38 m diameter.

General Simulation Strategy

Axi-symmetric cylindrical coordinates were assumed in the simulations. For all three sets of simulations 30 grid cells were used in the radial direction, 10 grid cells in the central core and 20 grid cells towards the wall region. Smaller sized cells were used in the bottom 0.2 m of the total column height. Non-uniform cells were used because we expect recirculatory liquid flows in the wall region and near the column bottom. An overview of the various grids used in the simulations is shown in Figure 26.

Both homogeneous and heterogeneous flow regimes were simulated. From the Reilly *et al.*[69] correlation it was determined that the superficial gas velocity at the regime transition point for the air-water system, $U_{trans} = 0.034\ \mathrm{m\,s^{-1}}$. For operation at $U < 0.034\ \mathrm{m\,s^{-1}}$, homogeneous bubbly flow regime was taken to prevail. For operation at $U > 0.034\ \mathrm{m\,s^{-1}}$, the complete three phase model was invoked. Following the model of Krishna and Ellenberger[3] we assume that in the churn-turbulent flow regime the superficial gas velocity through the small bubble phase is $U_{trans} = 0.034\ \mathrm{m\,s^{-1}}$. The remainder of the gas $(U - U_{trans})$ was taken to rise up the column in the form of large bubbles. This implies

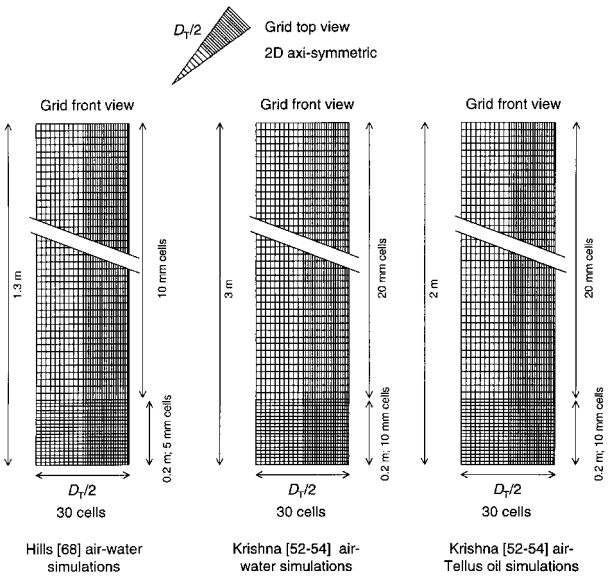

Figure 26. Computational grid for 2D axi-symmetric simulations.

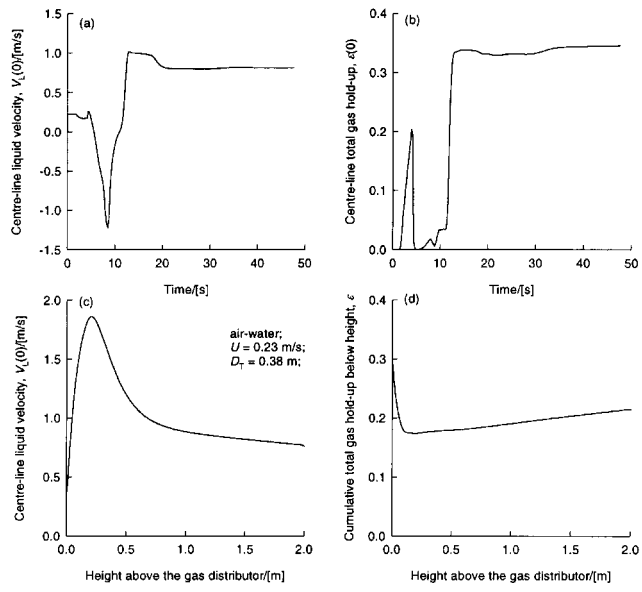

Figure 27. (a) and (b) show start-up dynamics for the centre-line liquid velocity and the centre-line gas hold-up for air-water simulation in a 0.38 m diameter column running with $U = 0.23\,\mathrm{m\,s^{-1}}$. (c) and (d) show the variation along the dispersion height in steady state.

that at the distributor the 'large' bubbles constitute a fraction $(U - U_{trans})/U$ of the total incoming volumetric flow, whereas the 'small' bubble constitute a fraction (U_{trans}/U) of the total incoming flow. To test the sensitivity of the results to assumption of the regime transition velocity, some simulations were also carried out taking $U_{trans} = 0.045\,\mathrm{m\,s^{-1}}$.

A further assumption made is that the formation of the large bubbles takes place immediately at the distributor; this is essentially a simplification and the justification for this is that our experimental studies show that the 'large' bubbles equilibrate within a distance of 0.1 m above the distributor[44]. The diamter of the 'small' bubbles was chosen as 4 mm in all the simulations. The injection of the small bubble phase was uniformly done over the central 24 of the 30 bottom grid cells. Based on visual observations of bubble column operation in the churn-turbulent flow regime, the large bubbles tend to concentrate in the central core. In order to reflect this the large bubble phase was injected over the central 13 of the 30 grid cells.

We also carried out 2D axi-symmetric simulations for the air-Tellus oil system. For the air-Tellus oil system, our dynamic gas disengagement experiments showed that the hold-up of the small bubble population was less than 2% and so we decided to ignore this presence of the small bubbles altogether in the CFD calculations. This is achieved by setting $U_{trans} = 0$. The hydrodynamics of air-Tellus oil system corresponds roughly to a situation in which large (spherical cap) bubbles rise through the column in a chain.

The time stepping strategy used in the transient simulations for attainment of steady state was typically: 20 steps at 5×10^{-4} s, 20 steps at 1×10^{-3} s, 460 steps at 5×10^{-3} s, 4500 steps at 1×10^{-2} s. The simulations were carried out on a Silicon Graphics Power Indigo workstation with an R8000 processor. Each simulation was completed in about 36 h. In all the runs steady state was reached within 40 s. Further details of the Eulerian simulations, including animations of the column start-up dynamics, are available on our web site: http://ct-cr4.chem.uva.nl/euler2D.

The simulations were started as follows. The column was initially filled with liquid to a specified height. At time $t = 0$, the gas was injected through the bottom distributor. The parameters such as velocities of phases and volume fractions were monitored at a specified height (in Figure 27 this height was 1.6 m above the distributor). A typical transient approach to steady-state is shown in Figure 27 for the 0.38 m diameter column operated with air-water at $U = 0.23\,\mathrm{m\,s^{-1}}$. When steady-state has been reached, the parameters at the end of the run were taken as steady-state values. The volume fractions and velocities were determined both at the monitoring height and along the column height. As can be seen in Figure 27, the centre-line liquid velocity $V_L(0)$ and cumulative gas hold-up ϵ do vary along the column height. In all cases the aspect ratios used in the simulations were about 5 or more and there was no significant difference between the gas hold-up below the monitoring height and that at the monitoring height itself. In the following, the distribution of velocities and volume fractions of the phases are reported at the monitoring height.

Simulations of Hills[68] Air-Water Experiments

The radial distributions of gas hold-up obtained with 2D simulations are compared in Figure 28 with the experimental data of Hills[68]. We note that the assumption of cylindrical axi-symmetry prevents lateral motion of the dispersed bubble phases and leads to an unrealistic gas bubble hold-up distribution wherein a maximum hold-up is experienced away from the central axis. Later in this paper, we shall see that a fully three-dimensional simulation will be required to get a proper representation of the gas hold-up distribution.

Figure 29 compares the gas hold-up averaged over the cross-section at a height of 0.6 m above the distributor from the 2D simulations with the experimental values of Hills[68]. We see that though the 2D axi-symmetric simulation predicts an unrealistic radial distribution of gas hold-up,

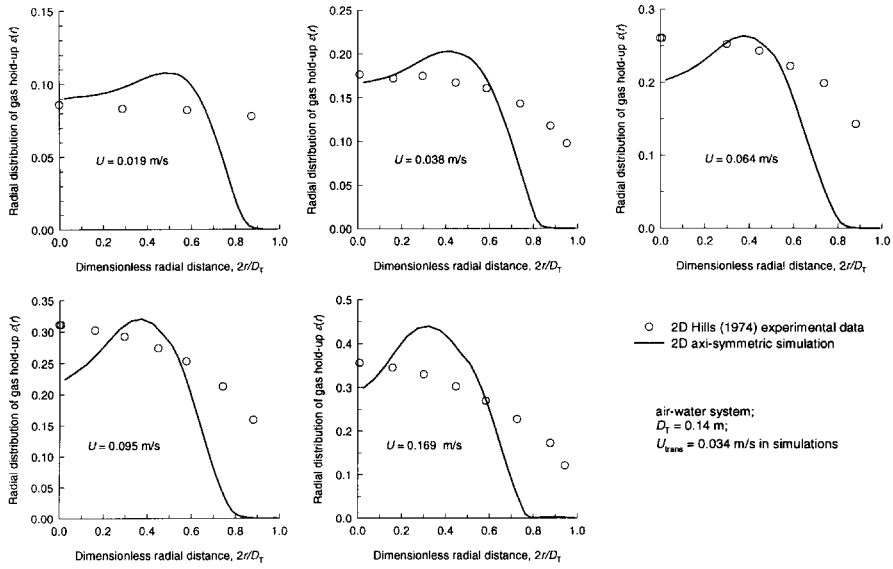

Figure 28. Comparison of radial profiles of gas hold-up obtained from 2D simulations of a 0.14 m diameter column for air–water system with experimental data of Hills[68]. Animations of the 2D simulations can be viewed our web site: http://ct-cr4.chem.uva.nl/euler2D

the prediction of the average gas hold-up is reasonably good. In order to emphasise the need for the including both 'large' and 'small' bubbles, we carried out simulations of the Hills experiments in which the 'large' bubbles were ignored, i.e. assuming that the dispersion was made up only of small bubbles. The simulated values of the gas hold-up are seen to be extremely high, at variance with the experiments; see Figure 29. Figure 30 compares the radial distribution of the axial component of the liquid velocity, obtained from the 2D simulations with experimental data of Hills[68]. The agreement must be considered to be very good when we realise that no fit parameters (expect perhaps U_{trans}) have been employed.

Simulations of Krishna *et al.*[52] Air-Water Experiments

Figure 31 compares the experimental data on total gas hold-up, and small bubble hold-up, with those from the simulations. We have shown simulation results both for $U_{trans} = 0.034$ and $0.045\ m\ s^{-1}$. Firstly, the right trends are followed by the simulations. Furthermore, it is clear that with a proper choice of U_{trans} a good match with experimental data can be obtained.

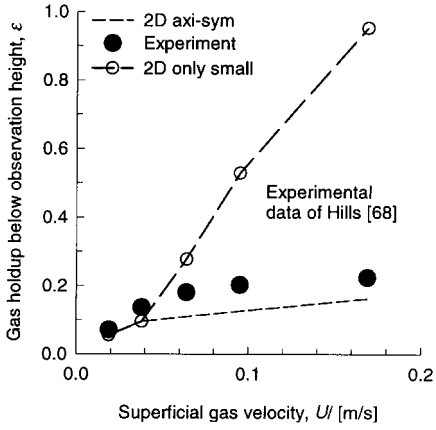

Figure 29. Comparison of experimental data of Hills[68] with Eulerian simulations for a range of superficial gas velocities: $U = 0.019, 0.038, 064, 0.095$ and $0.169\ m\ s^{-1}$. Also shown with dotted line are simulation results in which the dispersion is assumed to consist only of 4 mm sized small bubbles. The simulated values of the gas hold-up were determined by averaging the radial hold-up profile over the column cross section at a height of 0.6 m above the distributor.

The predictions of $V_L(0)$ from Eulerian simulations reflect the strong column diameter dependence, observed experimentally; see Figure 32. It is interesting to note that the choice of U_{trans} has little or no impact on the calculated $V_L(0)$ values. The match between simulated $V_L(0)$ and experimental data with varying U is reasonable and more accurate than most of the literature correlations. The Riquarts[70] correlation

$$V_L(0) = 0.21(gD_T)^{1/2}(U^3/g\nu_L)^{1/8} \quad (25)$$

represents the experimental data as well as our Eulerian simulations do.

The measurements of Krishna *et al.*[52] of the radial distribution of liquid velocity (axial component) $V_L(r)$, reflect the strong influence of the column diameter; see Figure 33. This column diameter influence is also reflected in the Eulerian simulations, shown on the right of the same figure. Figure 34 compares the normalised liquid velocity profile $V_L(r)/V_L(0)$ from 2D simulations with the experimental data of Krishna *et al.*[52] with air-water for a range of conditions for three columns. The CFD predictions are good, and certainly far superior to that of literature correlations for the normalised liquid velocity profile $V_L(r)/V_L(0)$.

Simulations of Krishna *et al.*[53,54] Air-Tellus Oil Experiments

The 2D simulations also give good agreement with the gas-hold-up and centre-line velocity data of Krishna *et al.*[53,54] for air-Tellus oil systems in three different columns; see Figures 35 and 36.

The experiments of Krishna *et al.*[53,54] in the 0.38 m diameter column with either water or Tellus oil show very

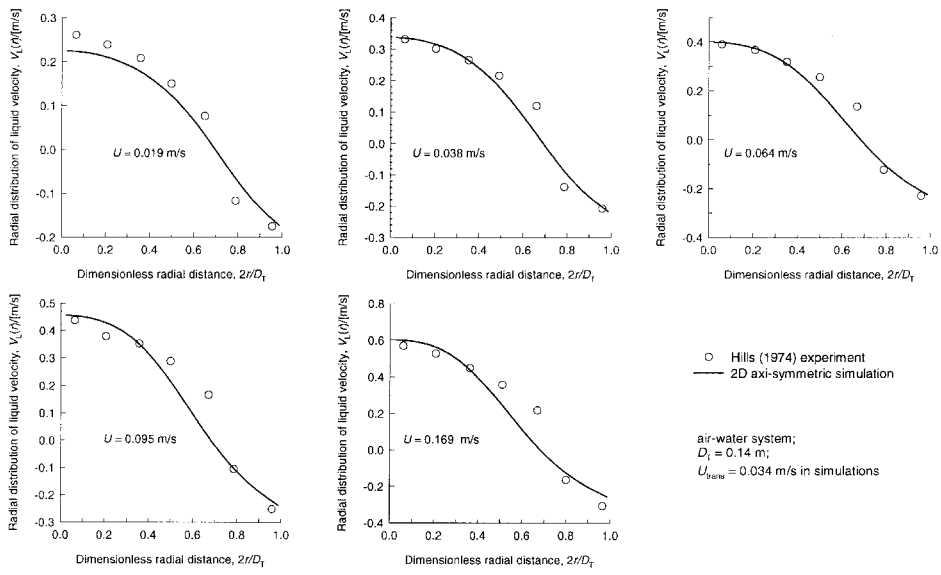

Figure 30. Radial distribution of liquid velocities at a height of 0.6 m above the distributor. Comparison between Eulerian simulations with experimental data of Hills[68].

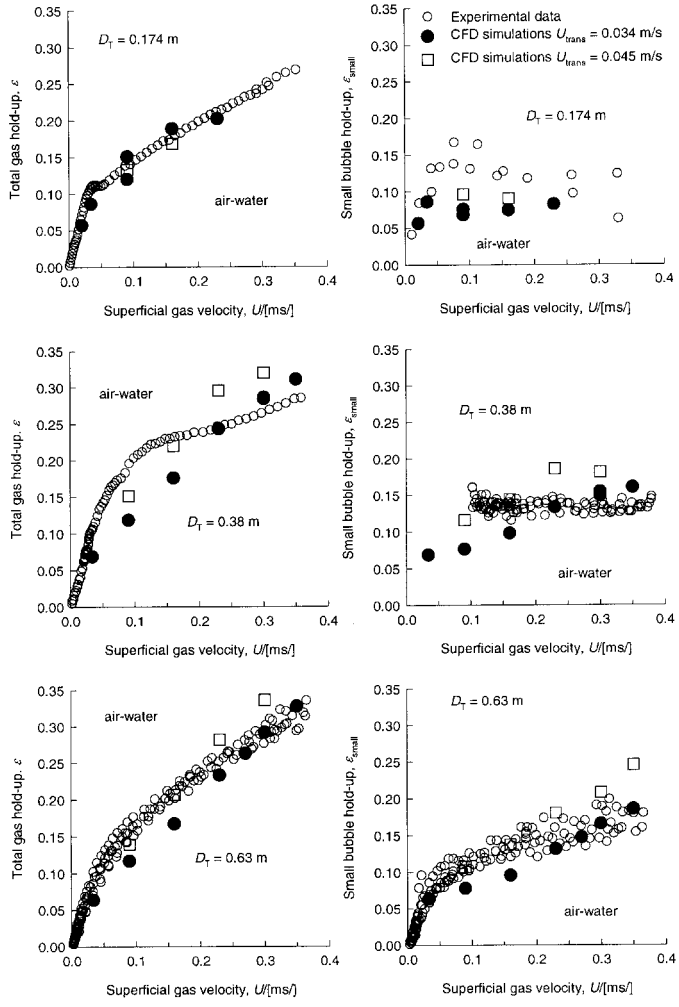

Figure 31. Comparison of experimental values of gas hold-up (total and small bubbles) with 2D Eulerian simulations with experimental data with air–water obtained by Krishna *et al.*[52–54].

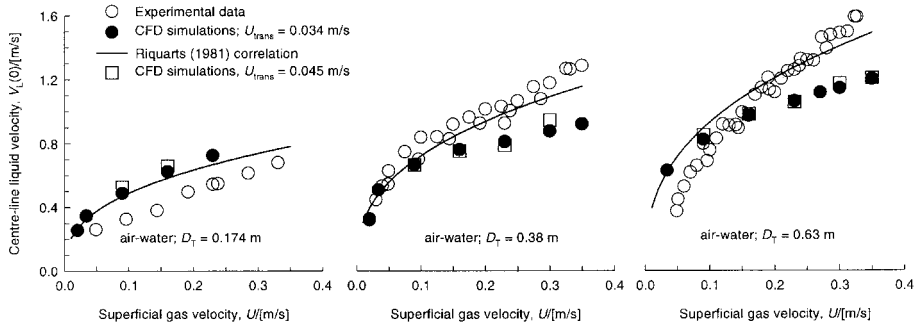

Figure 32. Comparison of experimental values of centre-line velocity $V_L(0)$ with 2D Eulerian simulations with experimental data with air–water obtained by Krishna *et al.*[52]. Also shown for comparison purposes is the Riquarts[70] correlation.

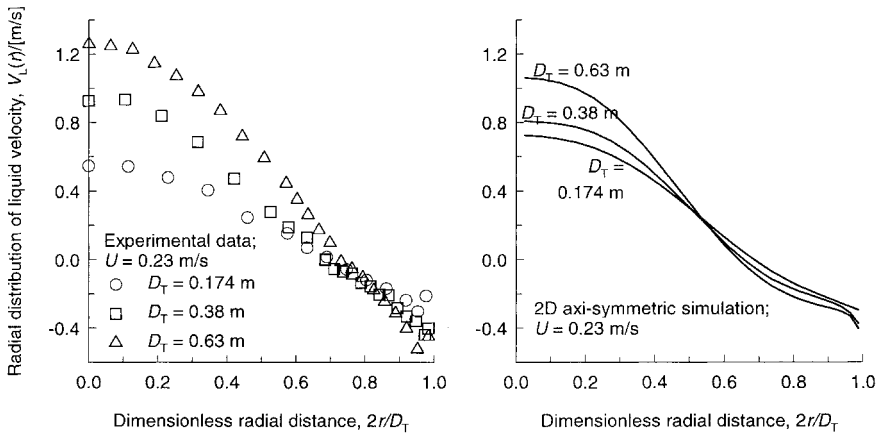

Figure 33. Comparison of radial profiles of liquid velocity obtained from 2D simulations with experimental data with air–water system at $U = 0.23\ \mathrm{m\,s^{-1}}$ for three different columns obtained by Krishna *et al.*[52].

little influence of liquid viscosity on $V_L(0)$; see Figure 36(a). The Eulerian simulations of $V_L(0)$ for water and Tellus oil systems give practically the same results for $V_L(0)$ over the superficial gas velocity range of 0.05–0.35 m s^{-1}, in broad agreement with experiment. Interestingly, the correlation of Riquarts[70] predicts a significantly lowering of $V_L(0)$ when the liquid viscosity is increased by a factor of 75, as is the case when we switch from water to Tellus oil. Use of Riquarts[70] correlation with the dynamic viscosity of water gives a much better representation the air-Tellus oil data. The radial distribution of liquid velocity $V_L(r)$ is practically identical for air-water and air-Tellus oil both in the experiments and in the 2D simulations; see Figure 36(b).

2D AXI-SYMMETRIC EULERIAN SIMULATIONS OF LARGE DIAMETER BUBBLE COLUMNS

Even for the air-water system, available literature correlations give significantly different results when considering scaling up to large column diameters. This is demonstrated by the predictions of the total gas hold-up for air-water and air-Tellus oil in Figures 4 and 5. The

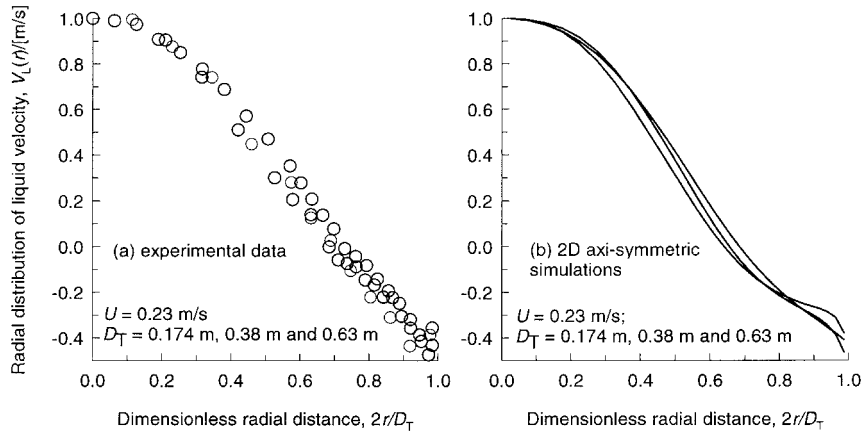

Figure 34. Normalised liquid velocity profiles $V_L(r)/V_L(0)$. Comparison between experiments of Krishna *et al.*[52] on the left with Eulerian simulations on the right.

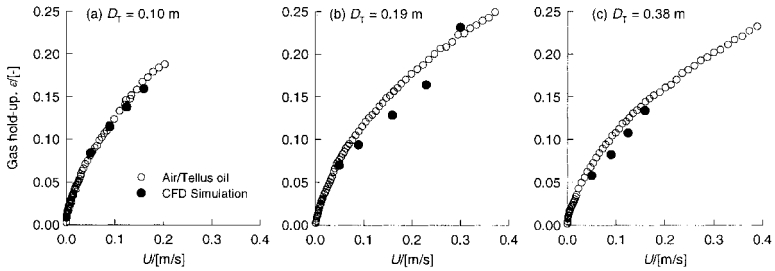

Figure 35. Comparison of experimental values of gas hold-up with air–Tellus oil system obtained by Krishna *et al.*[53,54] with Eulerian simulations. The simulated values of the gas hold-up are cumulative values below 1.6 m dispersion height.

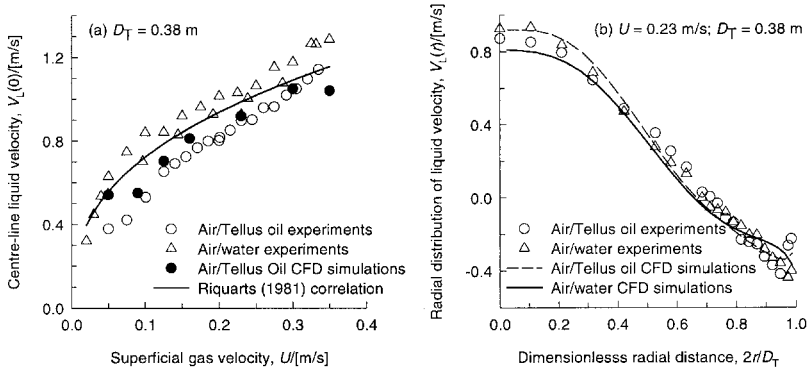

Figure 36. Comparison of experimental centre-line liquid velocity $V_L(0)$ and radial distribution $V_L(r)$ for air-Tellus oil and air-water with Eulerian simulations.

predictions of the centre-line liquid velocity $V_L(0)$ for air-water system, using a variety of literature correlations[70–78] is shown in Figure 37. We see from Figure 37 that the predictions of $V_L(0)$ for a bubble column of diameter 6 m diameter operating at $U = 0.3\,\mathrm{m\,s^{-1}}$ varies between 0.9 and $4.5\,\mathrm{m\,s^{-1}}$ using nine literature correlations. This represents a variation of a factor of five and so there is a clear need for a reliable scale up strategy. We shall use Eulerian simulations to predict the variation of hydrodynamic parameters of bubble columns with increasing column diameter.

Simulations were carried out for air–water and air–Tellus oil systems for column diameters ranging from 0.1 to 6 m, operating at two different superficial gas velocities, $U = 0.16$ and $0.30\,\mathrm{m\,s^{-1}}$. In all the simulations the column height to diameter ratio was kept at about five. For the 6 m diameter column the total column height was 35 m. Use of 10 mm grid cells, typically used in the simulations of small column diameters, is not practical. For columns larger than 2 m in diameter, we use 50 mm cells along the height. For the 6 m column, 35 m high, a total of $75 \times 710 = 53250$ cells were used. Grid convergence was confirmed even for 50 mm cells. Simulations of columns larger than 1 m were carried out on a Silicon Graphics Power Challenge machine with three R10000 processors running in parallel.

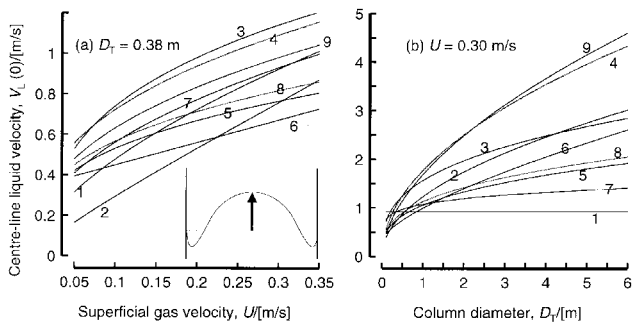

Figure 37. Comparison of literature correlations for the centre-line velocity $V_L(0)$ for air-water system. (a) Variation of $V_L(0)$ with superificial gas velocity for a column of 0.38 m diameter. (b) Variation of $V_L(0)$ with column diameter for a superficial gas velocity of $0.3\,\mathrm{m\,s^{-1}}$. The plotted correlations are: (1) Ohki and Inoue[75]; (2) Ueyama and Miyauchi[76]; (3) Joshi[72]; (4) Riquarts[70]; (5) Zehner[78]; (6) Nottenkämper *et al.*[74]; (7) Ulbrecht *et al.*[77]; (8) Kawase and Moo-Young[73]; (9) Bernemann[71].

The most dramatic expression of the scale effect is noticed when we compare the $V_L(r)$ as a function of the column diameter for a particular case, that of air-water operating at $U = 0.3\,\mathrm{m\,s^{-1}}$; see Figure 38. The centre-line velocity for the 6 m diameter column $V_L(0) = 4.5\,\mathrm{m\,s^{-1}}$. This goes part way toward choosing the proper correlation amongst the nine shown in Figure 37. When comparing air-water and air-Tellus oil simulations at the same value of U, we note that the liquid velocity distribution $V_L(r)$ is virtually the same; see Figure 39. A similar observation was reached earlier in Section 4.

For superficial gas velocities of 0.16 and $0.3\,\mathrm{m\,s^{-1}}$, Eulerian simulations were carried out to study the influence of column diameter. The results for air–water and air–Tellus oil are shown in Figures 40 and 41. For air–water system the predictions of $V_L(0)$ agree remarkably well with that of the Riquarts[70] correlation, Equation (25) and demonstrate extremely strong scale dependence. The Riquarts correlation can also be used for the air-Tellus oil results provided we use the kinematic viscosity of water. The data for both systems are compared to the Riquarts[70] correlation in Figure 42.

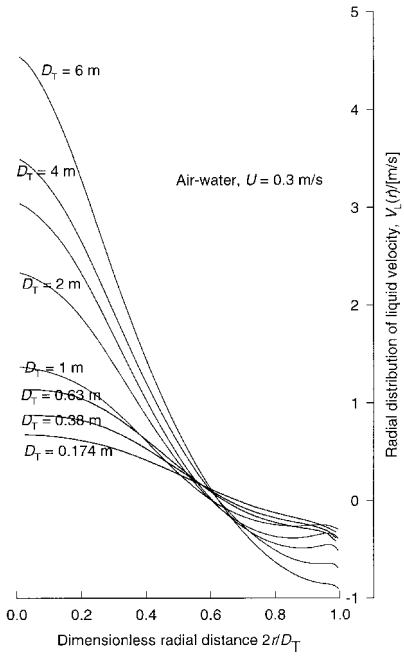

Figure 38. Scale effect on the radial distribution of liquid velocity.

Due to the strong liquid circulations with increasing column diameter, the bubbles will be accelerated. This acceleration effect causes a significant reduction in the large bubble hold-up with increasing column diameter; see Figures 40(a,b) and 41(a,b). Also shown are the calculations of the large bubble hold-up using the correlation of Krishna and Ellenberger[3]:

$$\epsilon_{b,large} = 0.268 \frac{1}{D_T^{0.18}} \frac{1}{(U - U_{trans})^{0.22}} (U - U_{trans})^{4/5} \tag{26}$$

where we have used $U_{trans} = 0$ for air–Tellus oil system.

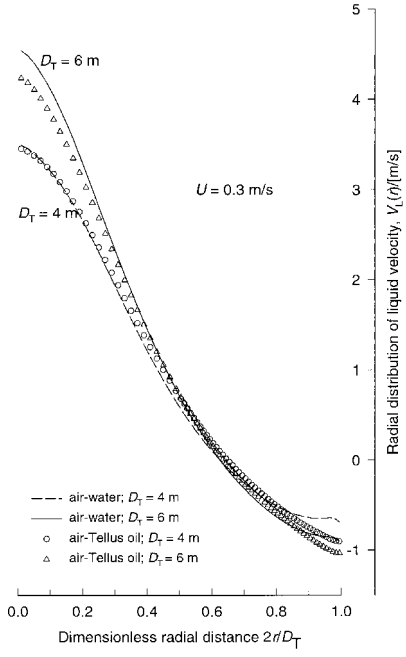

Figure 39. Comparison of air-water and air-Tellus oil simulations.

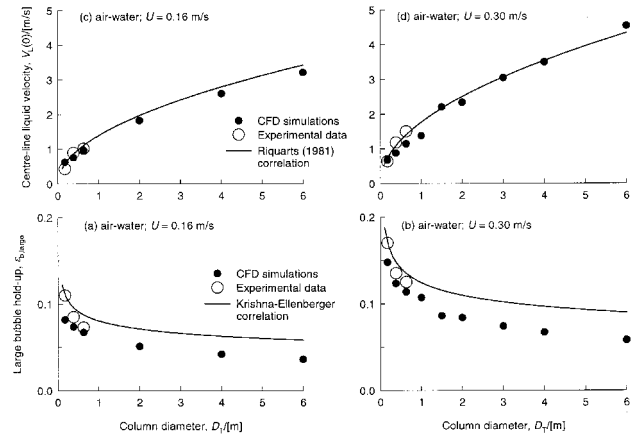

Figure 40. Influence of scale on the hold-up of large bubbles and on the centre-line liquid velocity for air-water.

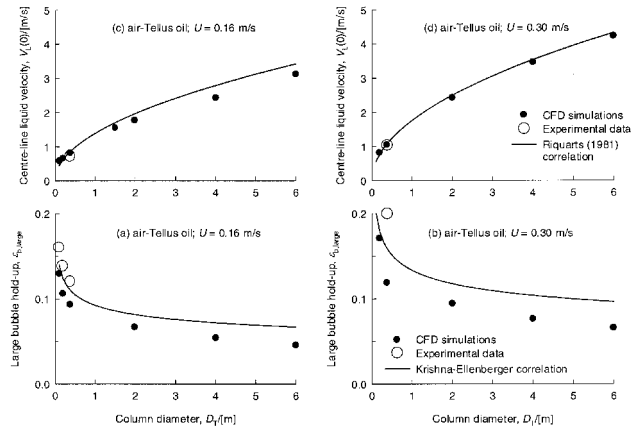

Figure 41. Influence of scale on the hold-up of large bubbles and on the centre-line liquid velocity for air-Tellus oil.

The decrease in the large bubble hold-up with column diameter from the Eulerian simulations is stronger than anticipated by Equation (26). Recent work[5,7] has shown that the scale up strategy advocated above for gas-liquid bubble columns can be applied to gas-solid fluidized beds.

3D SIMULATIONS OF BUBBLE COLUMNS

In reality, the hydrodynamics of a bubble column is chaotic in nature. Only the time-averaged profiles of volume fractions and velocities of the phases are axi-symmetric. At

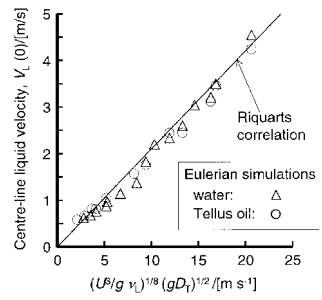

Figure 42. Comparison of Riquarts correlation (25) with Eulerian simulations for air-water and air-Tellus oil. We take $\nu_L = 10^{-6}$ m^2 s^{-1} for both water and Tellus oil, when applying Equation (25).

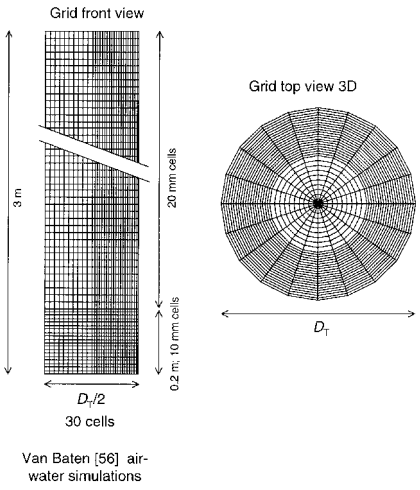

Figure 43. Sample grid for 0.38 m diameter column used for 3D simulations.

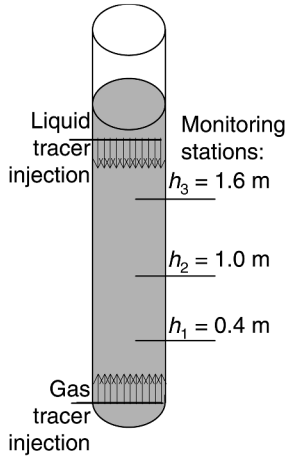

Figure 44. Liquid and gas phase tracer injection strategies in Eulerian simulations. The tracer concentrations are monitored at three stations over the entire cross-section.

any instant of time, the dispersion 'sloshes' from one side to the other. We will try to capture this behaviour by attempting fully three-dimensional simulation without imposing the constraint of axi-symmetry.

The computational grid used for the 0.38 m diameter column, 3 m tall column is shown, as an example, in Figure 43. Anticipating steeper velocity gradients near the wall region and in the bottom portion of the column, a non-uniform grid was used. In the radial direction 30 grid cells were used, 10 grid cells in the central core and 20 grid cells towards the wall region. In the axial direction the first 0.2 m bottom portion of the column consisted of 10 mm cells and the remainder 2.8 m height consisted of 20 mm cells. The total number of cells in the azimuthal direction was 20. The total number of cells was $30 \times 160 \times 20 = 96000$. An identical grid was used for the 0.174 and 0.63 m diameter columns. The gas injection policy was the same as in earlier sections.

The column was initial filled with pure liquid up to a height of say 1.8 m and the transient simulations were started with gas injection at time $t = 0$ s at the distributor plate. A typical time-stepping strategy for a 3D simulation was: 100 steps at 5×10^{-4} s, 100 steps at 1×10^{-3} s, 19800 steps at 5×10^{-3} s. Running on a Silicon Graphics Power Challenge machine employing three R10000 processors in parallel, this simulation took about 8 weeks to complete 20000 time steps. At the end of 11000 time steps, sufficient to attain quasi-steady state conditions, tracer was injected into the entering gas phase, uniformly over the whole cross-section, just above the bottom grid. At the same time step, liquid tracer was injected near the top of the dispersion, typically 2 m above the distributor plate. The transient responses of the gas and liquid phases were monitored over the entire grid cross-section at three monitoring stations, $h = 0.4$, 1 and 1.6 m above the distributor plate; see Figure 44.

The start-up dynamics of a typical 3D simulation are shown in Figure 45(a) and (b) for $V_L(0)$ and $\epsilon(0)$. The system evolves to a quasi-steady state. The variation of the time-averaged cumulative gas hold-up ϵ along the dispersion height is shown in Figure 45(c). Furthermore, the 3D simulation shows chaotic behaviour and this is illustrated by the snapshots of the liquid velocity and bubble hold-up profiles, at an arbitrary vertical plane through the centre of the column, at the three monitoring stations for three time steps, separated by 2.5 s; see Figure 46. The liquid sloshes from left to right and the chaotic motions can best be appreciated by viewing the animations on our web site http://ct-cr4.chem.uva.nl/oil-water. Figure 47 shows snapshots of the liquid velocity vectors at a height 1.6 m above the distributor for the same three time steps. The non-monotonic character of the liquid circulations is evident. The time- and azimuthal-averaged profiles for $h = 1.6$ m are shown in Figure 48. The time-averaged $V_L(r)$ is in good agreement with the measurements of Krishna *et al.*[52–54]. We note in Figure 48 that the small bubbles tend to concentrate

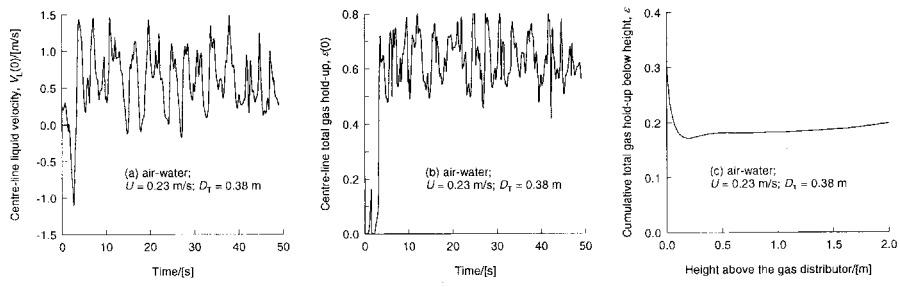

Figure 45. (a) and (b) show start-up dynamics for the centre-line liquid velocity and the centre-line gas hold-up for air-water simulation in a 0.38 m diameter column running with $U = 0.23$ m s^{-1}. (c) shows the variation of cumulative gas hold-up along the dispersion height.

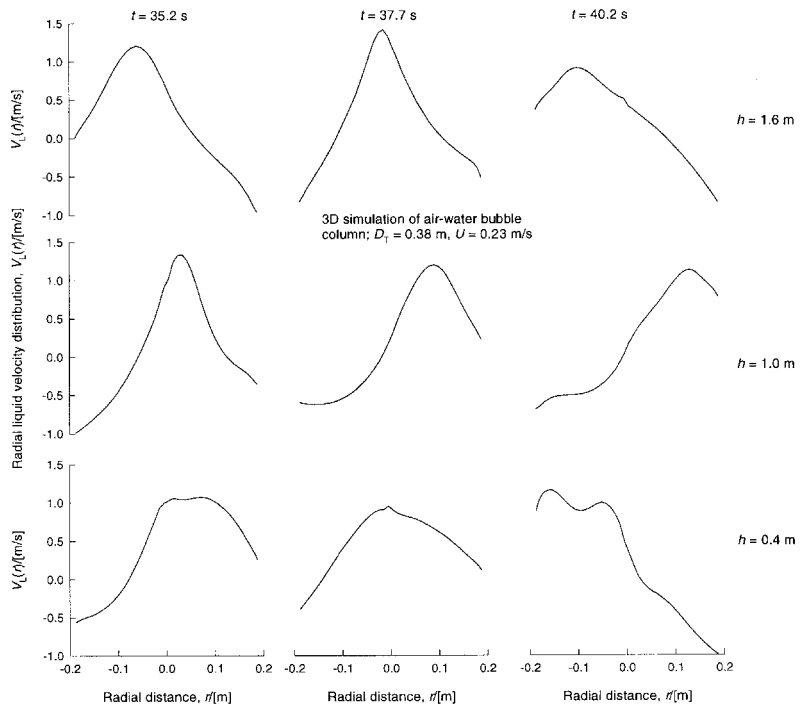

Figure 46. (a) Radial profiles of liquid velocity. Snapshots at three time steps and at the three monitoring stations in Figure 44. Column diameter = 0.38 m; air-water system, $U = 0.23\ \mathrm{m\,s^{-1}}$. The animations of this simulation can be viewed on our web site: http://ct-cr4.chem.uva.nl/oil-water

near the wall region whereas the large bubbles predominate in the central core.

The radial distribution of gas hold-up obtained with 2D and 3D simulations are compared in Figure 49(a)–(e) with experimental data of Hills[68] obtained in a 0.14 m diameter column. We note that the assumption of cylindrical axi-symmetry prevents lateral motion of the dispersed bubble phases and leads to an unrealistic gas bubble hold-up distribution wherein a maximum hold-up is experienced away from the central axis. The 3D simulations, on the other hand, in which lateral motion in both radial and azimuthal directions are catered for, yield physically realistic distribution of gas hold-ups, and are in reasonably good agreement with experiment. Recent work of Bauer and Eigenberger[47]

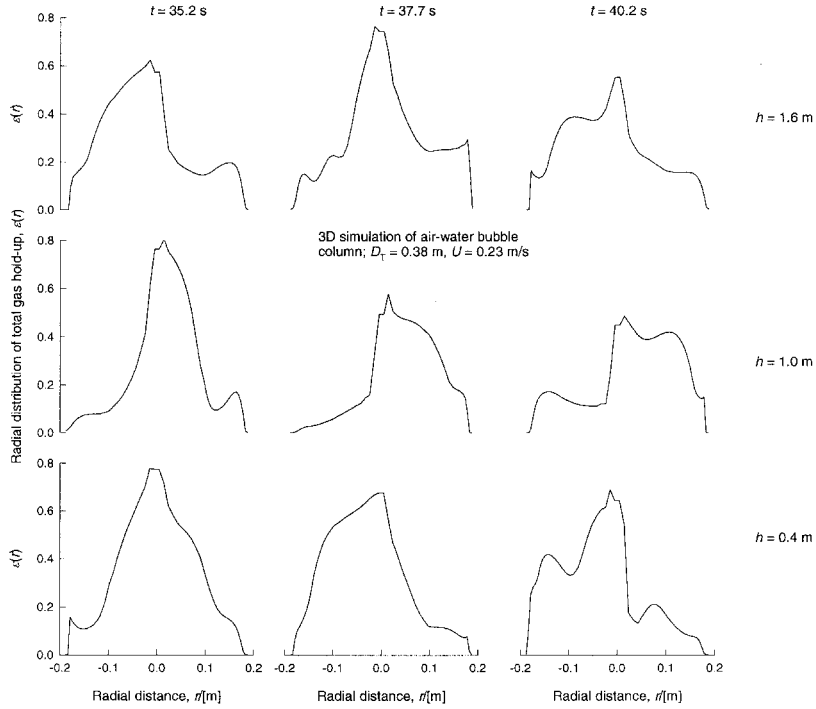

Figure 46. (b) Radial profiles of total gas hold-up. Snapshots at three time steps and at the three monitoring stations in Figure 44. Column diameter = 0.38 m; air-water system, $U = 0.23\ \mathrm{m\,s^{-1}}$. The animations of this simulation can be viewed on our web site: http://ct-cr4.chem.uva.nl/oil-water

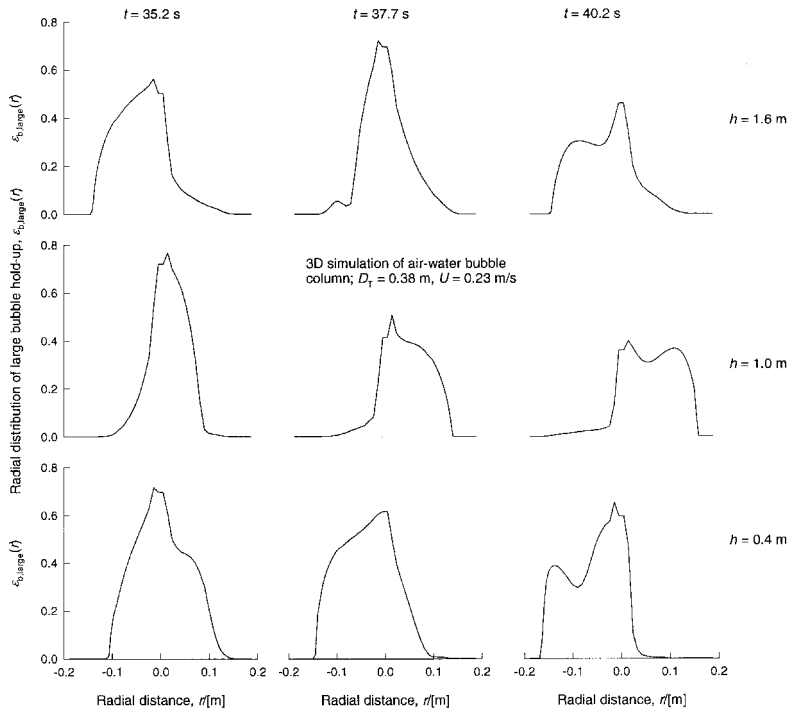

Figure 46. (c) Radial profiles of large bubble hold-up. Snapshots at three time steps and at the three monitoring stations in Figure 44. Column diameter = 0.38 m; air-water system, U = 0.23 m s^{-1}. The animations of this simulation can be viewed on our web site: http://ct-cr4.chem.uva.nl/oil-water

have underlined the impact of lateral fluxes of mass and momentum, resulting from 3D simulations, in the proper simulation of tracer dispersion.

Figure 50(a) compares the gas hold-up averaged over the cross-section at a height of 0.6 m above the distributor, from the simulations with the experimental values of Hills[68]. We see that though the 2D axi-symmetric simulation predicts an unrealistic radial distribution of gas hold-up, there is practically no difference between the 2D and 3D simulation results with respect to cross-section averaged hold-ups. The agreement with the experimental data of Hills[68] is reasonable, though the simulations tend to systematically

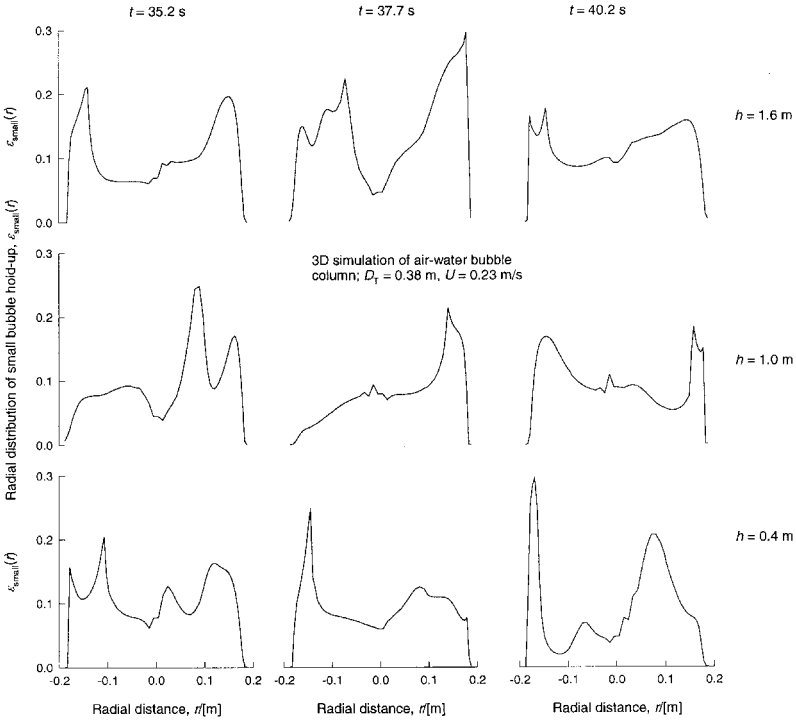

Figure 46. (d) Radial profiles of small bubble hold-up. Snapshots at three time steps and at the three monitoring stations in Figure 44. Column diameter = 0.38 m; air-water system, U = 0.23 m s^{-1}. The animations of this simulation can be viewed on our web site: http://ct-cr4.chem.uva.nl/oil-water

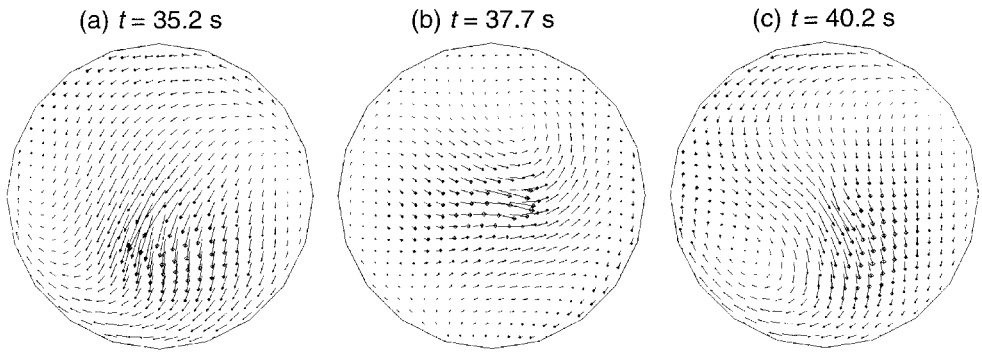

Figure 47. Snapshots of the liquid velocity vectors at a height 1.6 m above the distributor for three time steps for the 3D simulation of a 0.38 m diameter column with the air-water system operating at a superficial gas velocity of 0.23 m s^{-1}. Animations of the column start-up dynamics for the 2D and 3D simulations can be viewed on our web site: http://ct-cr4.chem.uva.nl/oil-water

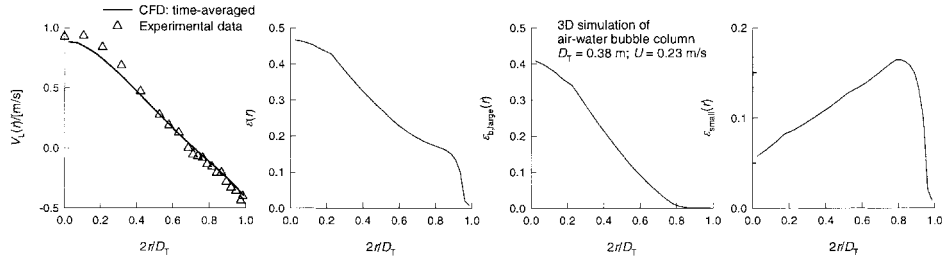

Figure 48. Time- and azimuthal-averaged radial profiles of liquid velocity (triangular symbols denote experimental data), total gas hold-up, large bubble hold-up and small bubble hold-up. Column diameter = 0.38 m; air-water system, U = 0.23 m s^{-1}.

under-predict the gas hold-up. In order to emphasise the need for the including both 'large' and 'small' bubbles, we carried out simulations of the Hills experiments in which the 'large' bubbles were ignored, i.e. assuming that the dispersion was made up only of small bubbles. The simulated values of the gas hold-up are seen to be extremely high, at variance with the experiments; see Figure 50(a). The cumulative values of the gas hold-ups (large + small) are plotted in Figure 50(b) as a function of the height above the distributor of a 0.38 m diameter column operating at U = 0.3 m s^{-1}. The cumulative gas hold-up values of the 2D and 3D simulations do not differ significantly and for a dispersion height of 1.6 m these values agree well with the experimentally determined value.

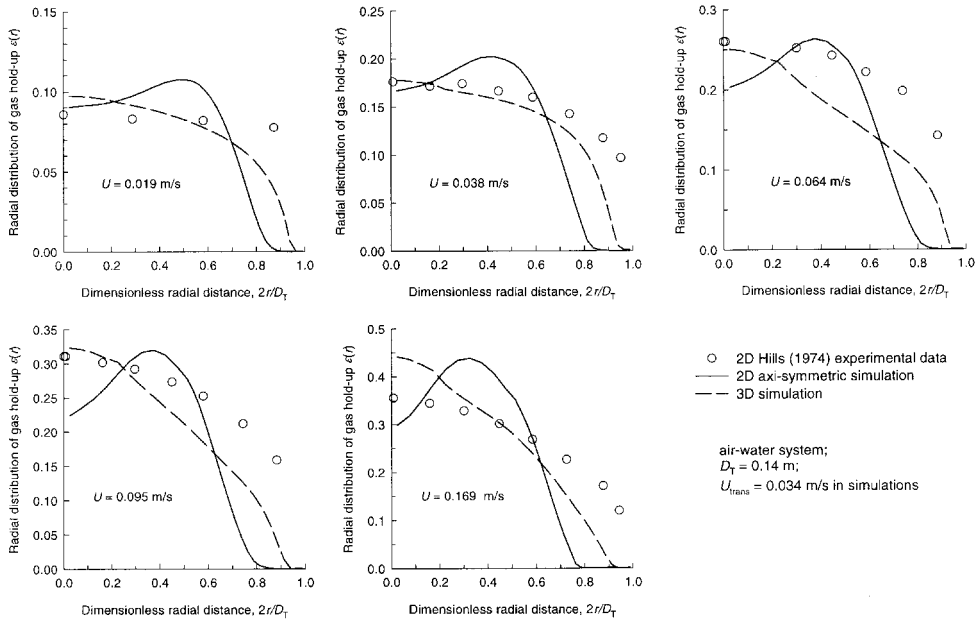

Figure 49. Comparison of radial profiles of gas hold-up obtained from 2D and 3D simulations of a 0.14 m diameter column for air-water system with experimental data of Hills[68]. Animations of the 2D and 3D simulations can be viewed on our web sites: http://ct-cr4.chem.uva.nl/euler2D and http://ct-cr4.chem.uva.nl/euler3D

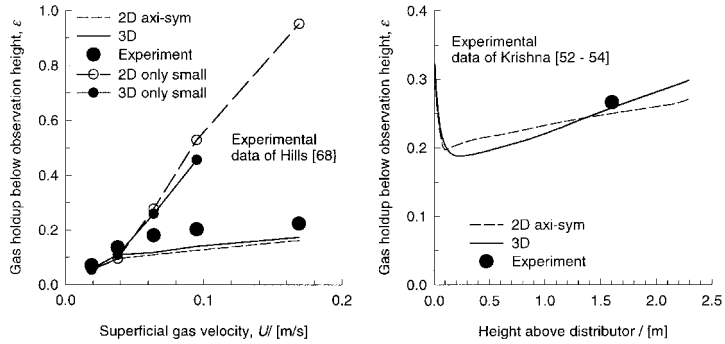

Figure 50. (a) Comparison of gas hold-ups obtained from 2D and 3D simulations of a 0.14 m diameter column with air–water system with experimental data of Hills[68]. Also shown are simulation results in which the dispersion is assumed to consist only of small bubbles. The gas hold-up value corresponds to the average at a height of 0.6 m above the distributor. (b) Cumulative gas hold-up for a 0.38 m diameter column operating at a superficial gas velocity of 0.3 m s^{-1}. The 2D and 3D simulation results are compared with each other. Also indicated in the figure is the experimentally measured value below a dispersion height of 1.6 m.

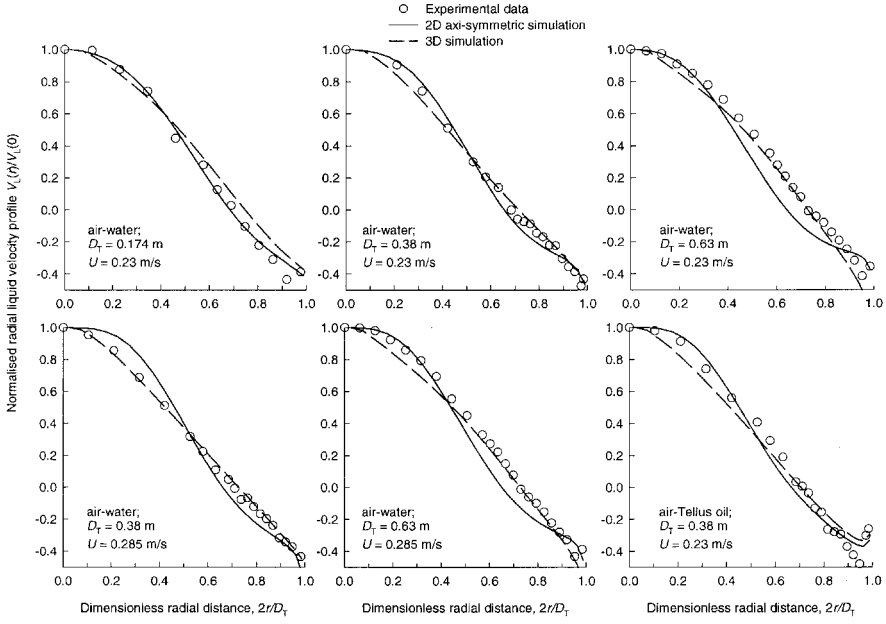

Figure 51. Comparison of normalised radial profiles of liquid velocity obtained from 2D and 3D simulations with experimental data with air–water system and air-Tellus oil by Krishna *et al.*[52–54].

Figure 51 compares the radial distribution of the axial component of the liquid velocity, normalised with respect to the centre-line velocity, $V_L(0)$, obtained from the 2D and 3D simulations with experiments of Krishna *et al.*[52–54] in columns of 0.174, 0.38 m and 0.63 m in diameter with air-water and air-Tellus oil. We see that both 2D and 3D simulated profiles are reasonably close to each other and are able to reproduce the experimental trends very well. For the larger diameter columns, 0.38 m and 0.63 m in diameter, operating at higher superficial gas velocity (U = 0.3 m/s) there are differences in the 2D and 3D simulated profiles of liquid velocity. The experimental data show that the 3D simulations have a better predictive character, as might be expected. The value of the centre-line liquid velocity predicted by the 2D and 3D simulations, monitored at a height 1.6 m above the distributor, are however close to each other. For example for the 0.38 m column operating at U = 0.3 m s^{-1}, $V_L(0)$ = 0.88 and 0.89 m s^{-1} for the 2D and 3D simulations respectively.

Figure 52 compares the experimental $V_L(r)$ profile for air-water and air–Tellus oil, measured by Krishna *et al.*[53,54] with the 3D simulations. Though the two liquids differ in viscosity by a factor 75, both experiments and 3D

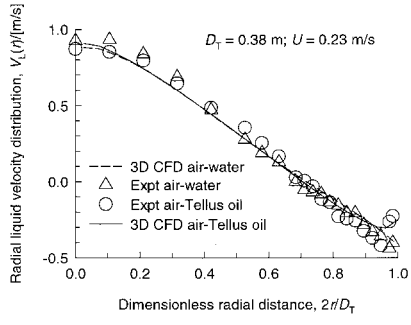

Figure 52. Time-averaged radial distribution of liquid velocity. Experimental data for air-water and air-Tellus oil compared with 3D Eulerian simulations.

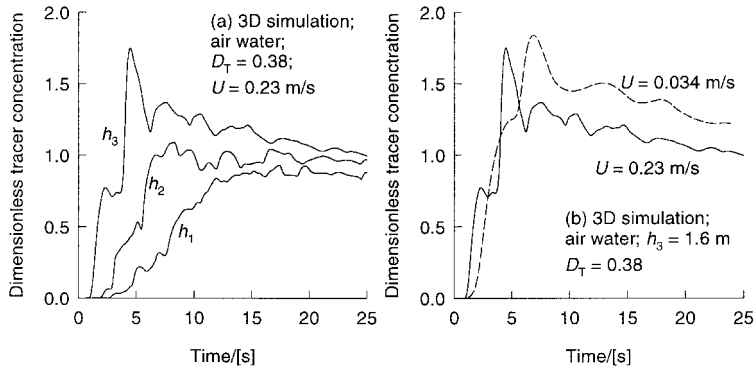

Figure 53. (a) Dimensionless tracer concentration in liquid phase from Eulerian simulations for air-water system in a column of 0.38 m diameter operating at $U = 0.23\ m\,s^{-1}$. (b) The tracer response for $U = 0.23\ m\,s^{-1}$ compared with that of a homogeneous run at $U = 0.034\ m\,s^{-1}$.

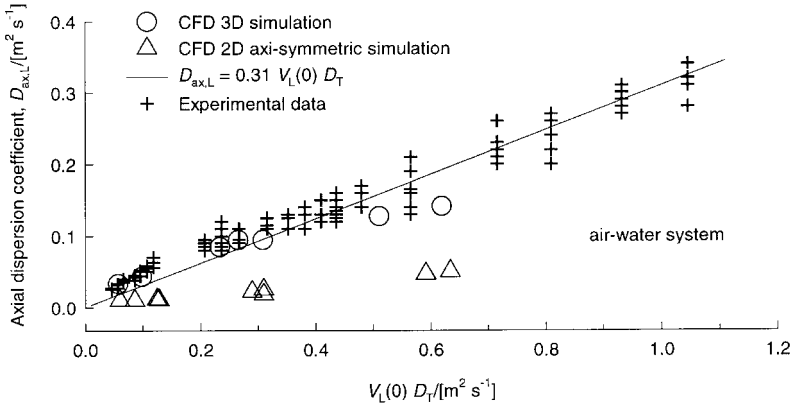

Figure 54. Axial dispersion coefficient of the liquid phase. Comparison of experimental data of Krishna *et al.*[54] with 2D and 3D Eulerian simulations.

simulations show almost no influence of liquid viscosity on the distribution $V_L(r)$.

Figure 53(a) shows a typical response to the liquid tracer injection from a 3D simulation. The responses at the three monitoring stations can be fitted to a one-dimensional axial dispersion model to obtain the value of $D_{ax,L}$. Figure 53(b) compares the response in the homogeneous flow regime ($U = 0.034\ m\,s^{-1}$) with that in the heterogeneous flow regime. The latter shows a much stronger dispersion. The values of $D_{ax,L}$ obtained by fitting the response curves shown in Figure 53(a) are compared with experimental data of Krishna *et al.*[52–54] in Figure 54. There is reasonably good agreement between the experimental data and the 3D simulations. Both conform to a simple empirical formula:

$$D_{ax,L} = 0.31\, V_L(0) D_T \tag{27}$$

which was derived earlier by Krishna *et al.*[52]. The 2D axi-symmetric simulations, however, yield $D_{ax,L}$ values about one order of magnitude lower than those found experimentally. This limitation of the 2D simulations to represent the mixing characteristics in bubble columns has been underlined earlier by Bauer and Eigenberger[47].

The response to the gas tracer experiments is shown in Figure 55, separately for (a) large bubbles, (b) small bubbles

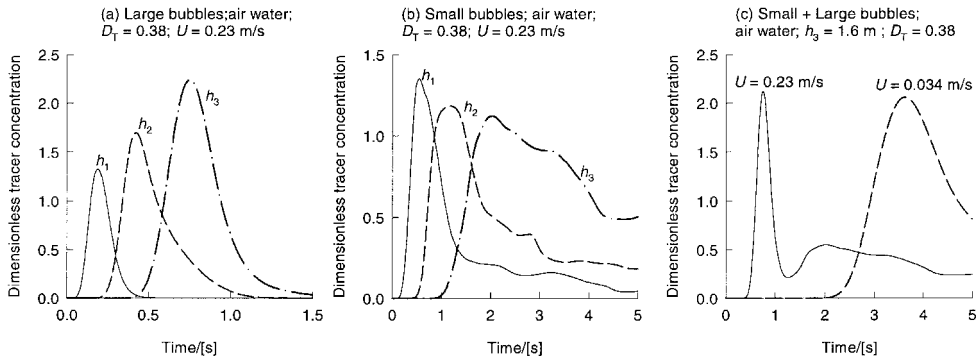

Figure 55. Dimensionless gas phase tracer concentrations a three monitoring positions. Eulerian simulations for 0.38 m diameter column. (a) Large bubble response, (b) small bubble response and (c) total gas response.

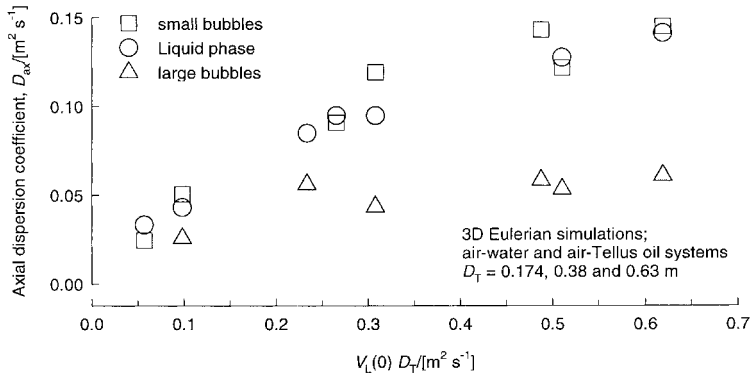

Figure 56. Axial dispersion coefficients of the liquid phase and gas phase (small and large bubbles).

and (c) total gas. In the churn-turbulent regime, the total gas RTD shows a camel-hump shaped curve, reported earlier in the experiments of Vermeer and Krishna[67]. Such a curve is not amenable to interpretation in terms of an axial dispersion model. Figure 55(c) shows clearly the differences between the gas phase RTD in the homogeneous (U = 0.034 m s^{-1}) and churn-turbulent flow regime. The responses of the large and small bubble populations, fitted separately to obtain $D_{ax,G,large}$ and $D_{ax,G,small}$, are compared with the simulated $D_{ax,L}$ values in Figure 56. The $D_{ax,G,small}$ are remarkably close to $D_{ax,L}$, this assumption has been incorporated into the bubble column slurry reactor model of Maretto and Krishna[79]. The dispersion of the large bubbles is significantly lower.

CONCLUDING REMARKS

Bubble column hydrodynamics is very complex and offers considerable challenges to the engineer during scale up. We have examined the utility of CFD as an investigative, design and scale-up tool. The following major conclusions can be drawn:

1. The Volume-of-Fluid (VOF) simulation technique is a powerful tool for studying the rise characteristics of single air bubbles in a column of liquid. Due to limitations of computer memory and speed, fully 3D simulations are not possible for 'meandering' bubbles smaller than about 12 mm in size because of the necessity to use grid cells of the order of a fraction of a millimetre. Therefore, only 2D simulations can be attempted. For 'small' bubbles in the 3–12 mm range, the bubble dynamics is qualitatively captured but the quantitative agreement with experiments in circular columns are not good.
2. VOF simulations of rise of spherical cap bubbles (corresponding to Eö > 40) in columns of circular cross-section are in excellent agreement with experiment. Similar excellent agreement is obtained when simulating the rise of circular cap bubbles in 2D rectangular columns.
3. A comparison of the VOF simulations and the Kinetic Theory of Granular Flow for fluidised solids, shows remarkable similarities in the rise characteristic of bubbles in liquids and beds of powders.
4. VOF simulations provide a powerful tool to study in-line interactions of pairs of spherical cap bubbles. This insight leads to the development of appropriate relations to predict the rise velocity of a swarm of large bubbles.
5. 2D axi-symmetric Eulerian simulations give a good representation of gas hold-up and centre-line liquid velocity, for both air-water and air-Tellus oil systems, for a range of column diameters.
6. The predictions of 2D axi-symmetric simulations for the radial distribution of gas hold-up are not realistic. The assumption of 2D axi-symmetry gives rise to an off-centre maximum in the gas hold-up.
7. Switching from water to Tellus oil as the liquid phase, with a factor 75 increase in the liquid viscosity, does not significantly affect either $V_L(0)$ or $V_L(r)$. This is found both experimentally and in 2D axi-symmetric simulations.
8. 2D axi-symmetric Eulerian simulations are useful for predicting the scale dependence of the centre-line velocity $V_L(0)$. Simulations show that $V_L(0)$ can approach values of about 4–5 m/s when the column diameter is increased to 6 m. The simulations further show that the liquid viscosity practically has no effect on $V_L(0)$. Based on Eulerian simulations we are able to recommend the use of the Riquarts correlation (25), provided we use the kinematic viscosity of water for all systems.
9. The strong increase in $V_L(0)$ with scale has the effect of accelerating the gas bubbles leading to significant reduction in the gas hold-up. The reduction in hold-up is significantly stronger than that anticipated by published literature correlations. Experimental data in the literature on gas hold-up and $V_L(0)$ in the churn-turbulent regime are restricted to columns smaller than 1 m in diameter. Therefore, there is a need for experimental verification with larger column diameters in order to verify the strong scale dependence anticipated by the Eulerian simulations.
10. For realistic predictions of radial distribution of liquid velocity and gas hold-up we must resort to fully three-dimensional Eulerian simulations.
11. For estimation of average gas hold-ups in the dispersion and circulating liquid velocities, typified by the centre-line velocity $V_L(0)$, 2D and 3D simulations are comparable. This is good news because the computational effort for 3D simulations is excessively large at the moment.
12. Both 2D and 3D simulations show a negligible influence of liquid viscosity on $V_L(r)$. This is in accord with experiment.

13. The liquid phase axial dispersion coefficients $D_{ax,L}$ predicted from 3D simulations are in good agreement with experiment. 2D axi-symmetric simulations lead to significantly lower predictions. Mixing processes are not properly captured when the constraint of axi-symmetry is imposed.
14. In the churn-turbulent regime, the total gas phase RTD is not amenable to interpretation in terms of an axial dispersion model. The individual bubble phase RTDs have to be fitted separately.
15. The small bubble axial dispersion coefficient $D_{ax,G,small}$ was found to be remarkably close in value to $D_{ax,L}$ suggesting that the small bubbles are 'entrained' with the liquid phase and have similar back-mixing characteristics. The dispersion of the large bubbles is significantly smaller.

Based on the evidence presented in this paper we suggest that CFD techniques are invaluable for design and scale up of bubble column reactors.

NOMENCLATURE

$c(\mathbf{X}, t)$	colour function, dimensionless
AF	wake acceleration factor, dimensionless
C_D	drag coefficient, dimensionless
d_b	diameter of either bubble population, m
d_p	particle size, m
D_{ax}	axial dispersion coefficient, $m^2\ s^{-1}$
D_T	column diameter, m
Eö	Eötvös number, $g(\rho_L - \rho_G)d_b^2/\sigma$
$\mathbf{F}_{sf}$	surface tension force, $N\ m^{-3}$
g	acceleration due to gravity, $9.81\ m\ s^{-2}$
H	dispersion height of the reactor, m
M	Morton number, $g\mu_L^4(\rho_L - \rho_G)/\rho_L^2\sigma^3$
$\boldsymbol{M}$	interphase momentum exchange term, $N\ m^{-3}$
n	Richardson-Zaki index, dimensionless
$\boldsymbol{n}$	vector normal to the interface, dimensionless
p	pressure, Pa
r	radial coordinate, m
Re	Reynolds number, $\rho_L d_b V_b/\mu_L$
SF	scale correction factor, dimensionless
t	time, s
U	superficial gas velocity, $m\ s^{-1}$
$\boldsymbol{u}$	velocity vector, $m\ s^{-1}$
U_{trans}	superficial gas velocity at regime transition, $m\ s^{-1}$
$(U - U_{trans})$	superficial gas velocity through the large bubbles, $m\ s^{-1}$
V_b	bubble rise velocity, $m\ s^{-1}$
$V_L(r)$	radial distribution of liquid velocity, $m\ s^{-1}$
$V_L(0)$	centre-line liquid velocity, $m\ s^{-1}$
$\boldsymbol{x}$	position coordinate, m
x	x-coordinate in cartesian geometry, m
z	axial coordinate, m
Δz	distance between leading and trailing bubbles, m

Greek symbols

α, β	parameters in eq. 17
$\epsilon_G \epsilon_L$	volume fraction of phase, dimensionless
ϵ	total gas hold-up, dimensionless
$\epsilon(r)$	radial distribution of total gas hold-up, dimensionless
$\epsilon(0)$	center-line total gas hold-up, dimensionless
ϵ_b	gas hold-up of large bubbles, dimensionless
ϵ_{trans}	gas hold-up at the regime transition point, dimensionless
$\kappa(\boldsymbol{x})$	curvature of bubble interface, dimensionless
μ	viscosity, Pa s
ν	kinematic viscosity of phase, $m^2\ s^{-1}$
ρ	density of phase, $kg\ m^{-3}$
σ	surface tension, N m
τ	viscous stress tensor, $N\ m^{-2}$

Subscripts

b	referring to bubble phase
G	referring to gas phase
k	phase, either L or G, small or large
l	referring to phase l
L	referring to liquid phase
large	referring to large bubbles
small	referring to small bubbles
trans	referring to regime transition point
T	tower or column

Superscripts

0	referring to a single isolated bubble

REFERENCES

1. Deckwer, W. D., 1992, *Bubble Column Reactors*, John Wiley & Sons, New York.
2. De Swart, J. W. A., Van Vliet, R. E. and Krishna, R., 1996, Size, structure and dynamics of 'large' bubbles in a 2-D slurry bubble column, *Chem Eng Sci*, 51: 4619–4629.
3. Krishna, R. and Ellenberger, J., 1996, Gas holdup in bubble column reactors operating in the churn-turbulent flow regime. *J AIChE*, 42: 2627–2634.
4. Krishna, R., Ellenberger, J. and Sie, S. T., 1996, Reactor development for conversion of natural gas to liquid fuels: A scale up strategy relying on hydrodynamic analogies. *Chem Eng Sci*, 51: 2041–2050.
5. Hoefsloot, H. C. J. and Krishna, R., 1993, Influence of gas density of flow regime transitions in homogenous flow in bubble columns, *Ind Eng Chem Res*, 32: 747–750.
6. Akita, K. and Yoshida, Y., 1973, Gas hold-up and volumetric mass-transfer coefficient in bubble columns. *Ind Eng Chem Proc Des Dev*, 12: 76–80.
7. Bach, H. F. and Pilhofer, T., 1978, Variation of gas hold-up in bubble columns with physical properties of liquids and operating parameters of columns, *Ger Chem Eng*, 1: 270–275.
8. Hikita, H., Asai, S., Tanigawa, K. and Kitao, M., 1980, Gas hold-up in bubble columns, *J Chem Eng*, 20: 59–67.
9. Hughmark, G. A., 1967, Hold-up and mass transfer in bubble columns, *Ind Eng Chem Proc Des Dev*, 6: 218–220.
10. Reilly, I. G., Scott, D. S., De Bruijn, T. J. W., Jain, A. K. and Piskorz, J., 1986, A correlation for gas hold-up in turbulent bubble column. *Can J Chem Eng*, 64: 705–717.
11. Wilkinson, P. M., Spek, A. P. and Van Dierendonck, L. L., 1992, Design parameters estimation for scale-up of high-pressure bubble columns, *J AIChE*, 38: 544–554.
12. Zehner, P., 1989, Mehrphasenströmungen in Gas-Flüssigkeits-Reaktoren, *Dechema Monogr*, 114: 215–233.
13. Clift, R., Grace, J. R. and Weber, M. E., 1978, *Bubbles, drops and particles*, Academic Press, San Diego.
14. Fan, L. S. and Tsuchiya, K., 1990, *Bubble wake dynamics in liquids and liquiid-solid suspensions*, Butterworth-Heinemann, Boston.
15. Delnoij, E., Kuipers, J. A. M. and Van Swaaij, W. P. M., 1997, Computational fluid dynamics applied to gas-liquid contactors, *Chem Eng Sci*, 52: 3623–3638.
16. Tomiyama, A., Zun, I., Sou, A. and Sakaguchi, T., 1993, Numerical analysis of bubble motion with the VOF method, *Nuclear Engineering and Design*, 141: 69–82.
17. Tomiyama, A., Sou, A., Minagawa, H. and Sakaguchi, T., 1993, Numerical analysis of a single bubble by VOF method. *JSME Int J, Series B*, 36: 51–56.
18. Tomiyama, A., 1998, Struggle with computational bubble dynamics, *Multiphase Science and Technology*, 10: 369–405.
19. Hirt, C. W. and Nichols, B. D., 1981, Volume of fluid (VOF) method for the dynamics of free boundaries, *J Comp Phys*, 39: 201–225.
20. Krishna, R., Urseanu, M. I., Van Baten, J. M. and Ellenberger, J., 1999, Rise velocity of a swarm of large gas bubbles in liquids, *Chem Eng Sci*, 54: 171–183.
21. Krishna, R. and Van Baten, J. M., 1999, Simulating the motion of gas bubbles in a liquid, *Nature*, 398: 208.
22. Krishna, R., Urseanu, M. I., Van Baten, J. M. and Ellenberger, J., 1999, Wall effects on the rise of single gas bubbles in liquids, *Int Commn Heat Mass Transfer*, 26: 781–790.
23. Krishna, R. and Van Baten, J. M., 2000, Simulating the Rise Characteristics of Gas bubbles in Liquids using Computational Fluid Dynamics, *Chem Eng Technol*, 24: 427–430.
24. Krishna, R. and Van Baten, J. M., 1999, Rise characteristics of gas bubbles in a 2D rectangular column: VOF simulations vs experiments, *Int Comm Heat Mass Transfer*, 26: 965–974.

25. Krishna, R., Van Baten, J. M., Urseanu, M. I., Ellenberger, J., 2000, Rise Velocity of Single Circular-Cap Bubbles in Two-dimensional Beds of Powders and Liquids, *Chem Eng & Proc*, 39: 433–440.
26. Krishna, R., 2000, A scale up strategy for a commercial scale bubble column slurry reactor for Fischer Tropsch synthesis, *Oil & Gas Science and Technology, Revue de L'Institut Francais du Petrole*, 55: 359–393.
27. Brackbill, J. U., Kothe, D. B. and Zemarch, C., 1992, A continuum method for modelling surface tension, *J Comp Phys*, 100: 335–354.
28. Harmathy, T. Z., 1960, Velocity of large drops and bubbles in media of infinite or restricted extent, *J AIChE*, 6: 281–288.
29. Richardson, J. F. and Zaki, W. N., 1954, Sedimentation and fluidisation: Part I, *Trans Inst Chem Eng*, 32: 35–53.
30. Davies, R. M. and Taylor, G. I., 1950, The mechanics of large bubbles rising through extended liquids and through liquids in tubes, *Proc Roy Soc London*, A200: 375–390.
31. Collins, R., 1967, The effect of a containing cylindrical boundary on the velocity of a large gas bubble in a liquid, *J Fluid Mech*, 28: 97–112.
32. Davidson, J. F., Harrison, D., Darton, R. C. and LaNauze, R. D., 1977, The two-phase theory of fluidization and its application to chemical reactors. in *Chemical Reactor Theory, A Review*, Lapidus, L. and Amundson, N. R. (Eds), Prentice-Hall, Englewood Cliffs, New Jersey, 583–685.
33. Geldart, D. (Ed), 1986, *Gas Fluidization Technology*, John Wiley, New York.
34. Mudde, R. F., Schulte, H. B. M. and Van den Akker, H. E. A., 1994, Analysis of a bubbling 2-D gas-fluidized bed using image-processing, *Powder Technology*, 81: 149–159.
35. Boemer, A., Qi, H. and Renz, U., 1997, Eulerian simulation of bubble formation at a jet in a two-dimensional fluidized bed, *Int J Multiphase Flow*, 23: 927–944.
36. Ding, J. and Gidaspow, D., 1990, A bubbling fluidization model using the kinetic theory of granular flow, *J AIChE*, 36: 523–538.
37. Fan, L. S. and Zhu, C., 1997, *Principles of Gas-Solid Flows*, Cambridge University Press, Cambridge.
38. Gidaspow, D., 1994, *Multiphase flow and fluidization–Continuum and kinetic theory descriptions*, Academic Press, San Diego.
39. Jenkins, J. T. and Savage, S. B., 1983, A theory for the rapid flow identical, smooth, nearly elastic spherical particles, *J Fluid Mech*, 130: 187–202.
40. Kuipers, J. A. M., Van Duin, K. J., Van Beckum, F. P. H. and Van Swaaij, W. P. M., 1992, A numerical model of gas fluidized beds, *Chem Eng Sci*, 47: 1913–1924.
41. Syamlal, M. and O'Brien, T. J., 1989, Computer simulation of bubbles in a fluidized bed. *AIChE Symposium Series No. 270*, 85: 22–31.
42. Van Wachem, B. G. M., Schouten, J. C., Krishna, R. and Van den Bleek, C. M., 1998, Eulerian simulations of bubbling behaviour in gas-solid fluidized beds, *Computers and Chemical Engineering*, 22: S299–S306.
43. Van Wachem, B. G. M., Schouten, J. C., Krishna, R. and Van den Bleek, C. M., 1999, Validation of the Eulerian simulated dynamic behaviour of gas-solid fluidised beds, *Chem Eng Sci*, 54: 2141–2149.
44. Ellenberger, J. and Krishna, R., 1994, A unified approach to the scale-up of gas-solid fluidized and gas-liquid bubble column reactors, *Chem Eng Sci*, 49: 5391–5411.
45. Krishna, R. and Ellenberger, J., 1995, A unified approach to the scale-up of 'fluidized' multiphase reactors, *Chem Eng Res Des*, 73: 217–221.
46. Krishna, R., Van Baten, J. M. and Ellenberger, J., 1998, Scale effects in fluidized multiphase reactors, *Powder Technology*, 100: 137–146.
47. Bauer, M. and Eigenberger, G., 1999, A concept for multi-scale modeling of bubble columns and loop reactors, *Chem Eng Sci*, 54: 5109–5117.
48. Boisson, N. and Malin, M. R., 1996, Numerical prediction of two-phase flow in bubble columns. *Int J Numerical Methods in Fluids*, 23: 1289–1310.
49. Grevskott, S., Sannæs, B. H., Dudukovic, M. P., Hjarbo, K. W. and Svendsen, H. F., 1996, Liquid circulation, bubble size distributions, and solids movement in two- and three-phase bubble columns, *Chem Eng Sci*, 51: 1703–1713.
50. Grienberger, J. and Hofmann, H., 1992, Investigations and modelling of bubble columns. *Chem Eng Sci*, 47: 2215–2220.
51. Jakobsen, H. A., Sannæs, B. H., Grevskott, S., and Svendsen, H. F., 1997, Modeling of bubble driven vertical flows, *Ind Eng Chem Res*, 36: 4052–4074.
52. Krishna, R., Urseanu, M. I., Van Baten, J. M. and Ellenberger, J., 1999, Influence of scale on the hydrodynamics of bubble columns operating in the churn-turbulent regime: Experiments vs Eulerian simulations, *Chem Eng Sci*, 54: 4903–4911.
53. Krishna, R., Van Baten, J. M. and Urseanu, M. I., 2000, Three-phase Eulerian simulations of bubble column reactors operating in the churn-turbulent flow regime: A scale up strategy, *Chem Eng Sci*, 55: 3275–3286.
54. Krishna, R., Urseanu, M. I., van Baten, J. M., Ellenberger, J., 2000, Liquid phase dispersion in bubble columns operating in the churn-turbulent flow regime, *J Chem Eng*, 78: 43–51.
55. Krishna, R., Van Baten, J. M., Urseanu, M. I., Ellenberger, J., 2001, Design and scale-up of the bubble column slurry reactor for Fischer-Tropsch synthesis, *Chem Eng Sci*, 56: 537–545.
56. Van Baten, J. M. and Krishna, R., 2001, Eulerian simulations for determination of the axial dispersion of liquid and gas phases in bubble columns operating in the churn-turbulent regime, *Chem Eng Sci*, 56: 503–512.
57. Krishna, R. and Van Baten, J. M., 2001, Using CFD for scaling up gas-solid bubbling fluidised bed reactors with Geldart A powders, *J Chem Eng*, 82: 247–257.
58. Krishna, R., Van Baten, J. M., Urseanu, M. I., Ellenberger, J., 1999, A scale up strategy for bubble column slurry reactors, *Catalysis Today*, 66: 199–207.
59. Krishna, R., Van Baten, J. M., Urseanu, M. I., 2001, Scale effects on the hydrodynamics of bubble columns operating in the homogeneous flow regime, *Chem Eng Tech*, 24: 451–458.
60. Lapin, A. and Lübbert, A., 1994, Numerical simulation of the dynamics of two-phase gas-liquid flows in bubble columns, *Chem Eng Sci*, 49: 3661–3674.
61. Sanyal, J., Vasquez, S., Roy, S. and Dudukovic, M. P., 1999, Numerical simulation of gas-liquid dynamics in cylindrical bubble column reactors, *Chem Eng Sci*, 54: 5071–5083.
62. Sokolichin, A. and Eisenberger, G., 1994, Gas-liquid flow in bubble columns and loop reactors: Part I. Detailed modelling and numerical simulation, *Chem Eng Sci*, 49: 5735–5746.
63. Sokolichin, A. and Eigenberger, G., 1999, Applicability of the standard–turbulence model to the dynamic simulation of bubble columns: Part I. Detailed numerical simulations, *Chem Eng Sci*, 2273–2284.
64. Torvik, R. and Svendsen, H. F., 19990, Modelling of slurry reactors. A fundamental approach, *Chem Eng Sci*, 45: 2325–2332.
65. Delnoij, E., Lammers, F. A., Kuipers, J. A. M. and Van Swaaij, W. P. M., 1997, Dynamic simulation of dispersed gas-liquid two-phase flow using a discreet bubble model, *Chem Eng Sci*, 52: 1429–1458.
66. Sokolichin, A., Eigenberger, G., Lapin, A. and Lübbert, A., 1997, Direct numerical simulation of gas-liquid two-phase flows, Euler/Euler versus Euler/Lagrange, *Chem Eng Sci*, 52: 611–626.
67. Vermeer, D. J. and Krishna, R., 1981, Hydrodynamics and mass transfer in bubble columns operating in the churn-turbulent regime, *Ind Eng Chem Proc Des & Dev*, 20: 475–482.
68. Hills, J. H., 1974, Radial non-uniformity of velocity and voidage in a bubble column, *Chem Eng Res Des*, 52: 1–9.
69. Reilly, I. G., Scott, D. S., De Bruijn, T. J. W. and MacIntyre, D., 1994, The role of gas phase momentum in determining gas holdup and hydrodynamic flow regimes in bubble column operations, *Can J Chem Eng*, 72: 3–12.
70. Riquarts, H. P., 1981, Strömungsprofile, Impulsaustausch und Durchmischung der flüssigen Phase in Bläsensaulen, *Chem Ing Tech*, 53: 60–61.
71. Bernemann, K., 1989, Zur Fluiddynamik und zum Vermischungsverhalten der flüssigen Phase in Blasensäulen mit längsangeströmten Rohrbundeln. *PhD Thesis, University Dortmund.*
72. Joshi, J. B., 1980, Axial mixing in multiphase contactors–A unified correlation, *Chem Eng Res Des*, 58: 155–165.
73. Kawase, Y. and Moo-Young, M., 1989, Turbulent intensity in bubble column, *Chem Eng*, 40: 55–58.
74. Nottenkämper, R., Steiff, A. and Weinspach, P. M., 1983, Experimental investigation of hydrodynamics of bubble columns, *Ger Chem Eng* 6: 147–155.
75. Ohki, Y. and Inoue, H., 1970, Longitudinal mixing of the liquid phase in bubble columns, *Chem Eng Sci*, 25: 1–16.
76. Ueyama, K. and Miyauchi, T., 1979, Properties of recirculating turbulent two phase flow in gas bubble columns, *J AIChE*, 25: 258–266.
77. Ulbrecht, J. J., Kawase, Y. and Auyeung, K. F., 1985, More on mixing of viscous liquids in bubble columns, *Chem Eng Comm*, 35: 175–191.
78. Zehner, P., 1986, Momentum, mass and heat transfer in bubble columns. Part 1. Flow model of the bubble column and liquid velocities, *Int Chem Eng*, 26: 22–35.

79. Maretto, C. and Krishna, R., 1999, Modelling of a bubble column slurry reactor for Fischer Tropsch synthesis, *Catalysis Today*, 52: 279–289.

ACKNOWLEDGEMENTS

Financial assistance from The Netherlands Foundation for Scientific Research (NWO) in the form of a 'programmasubsidie' to RK is gratefully acknowledged. JMvB is also grateful to NWO for grant of a PhD fellowship.

ADDRESS

Correspondence concerning this paper should be addressed to Professor R. Krishna, Department of Chemical Engineering, University of Amsterdam, Nieuwe Achtergracht 166, 1018 WV Amsterdam, The Netherlands. Fax: +31 20 525 504. E-mail: krishna@its.chem.uva.nl

The manuscript was received 7 June 2000 and accepted for publication after revision 20 April 2001.